

Generalized many-body perturbation theory for the electron correlation energy

Yuqi Wang, Wei-Hai Fang, and Zhendong Li*

Key Laboratory of Theoretical and Computational Photochemistry, Ministry of Education,
College of Chemistry, Beijing Normal University, Beijing 100875, China

Standard many-body perturbation theory (MBPT) using a quadratic zeroth-order Hamiltonian is a cornerstone of many *ab initio* computational methods for molecules and materials. However, this perturbation expansion can break down in the presence of strong electron correlation, which occurs in many scenarios such as the bond dissociation of molecules in chemical reactions. In this work, we developed a generalized (time-dependent) MBPT for computing electron correlation energies, in which the zeroth-order Hamiltonian can be interacting and hence the zeroth-order reference state is a multi-determinant wavefunction instead of a single Slater determinant in general. This allows us to take strong correlation into account from the outset and treat the residual weak interaction by diagrammatic perturbation expansion. Using this framework, we formulated a multi-reference (MR) generalization of the standard single-reference (SR) random phase approximation (RPA) for the electron correlation energy by resumming generalized ring diagrams including cumulant contributions, which naturally leads to a set of unified equations that work in both SR and MR cases. To further include exchange effects, we also derived a multi-reference second-order screened exchange (SOSEX) correction from a coupled-cluster perspective of the resulting MR-RPA. Applications to prototypical molecules demonstrate that MR-RPA/SOSEX successfully resolves the well-known failure of the conventional SR-RPA/SOSEX for molecular dissociation. Our work bridges MBPT in condensed matter physics and multi-reference perturbation theory in quantum chemistry, opening up new possibilities for advancing computational methods for the electron correlation energy via diagrammatic resummation.

Introduction.— Electron correlation plays a pivotal role in determining the electronic properties of molecules and materials. Understanding electron correlation within many-electron systems through *ab initio* calculations remains a fundamental challenge in modern quantum physics and chemistry[1–3]. Many-body perturbation theory (MBPT) provides a rigorous framework to develop useful computational methods for studying electron correlation[4, 5]. Among them, random phase approximation (RPA)[6, 7] represents one of the simplest methods, which includes certain type of Feynman diagrams to infinite order[8]. Originally developed for interacting electron gas, RPA has nowadays been widely used to compute the electron correlation energy for molecules and materials[9–12]. It has also aroused substantial theoretical interests for further improving the accuracy by combining with density functional theory (DFT) via the adiabatic connection fluctuation-dissipation (ACFDT) theorem[13–17], including exchange effects[18–21] as well as single-excitation corrections[22], connecting to coupled cluster (CC) theory[23–26], and choosing different two-particle interaction channels[27, 28]. These developments have significantly deepened our understanding of electron correlation in complex systems.

Despite the great successes of methods based on standard MBPT for weakly correlated systems, they often fail miserably in the presence of strong electron correlation, where the perturbation series typically breaks down. This failure can be found in many important applications such as stretching and breaking of chemical bonds, as documented in recent works for RPA and *GW*[29, 30]. The failure of standard MBPT for strong correlation can

be attributed to the use of a single Slater determinant as the reference state and a quadratic mean-field Hamiltonian as the zeroth-order Hamiltonian \hat{H}_0 .

In this Letter, we develop a generalized MBPT, which allows us to use an interacting zeroth-order Hamiltonian and a multi-determinant reference that treat strong correlation to infinite order from the outset. The residual weak interaction can be added by a generalized diagrammatic expansion similar to standard MBPT. Using this framework, we formulated a multi-reference (MR) generalization of RPA and the second-order screened exchange (SOSEX)[18] approaches. Compared with previous efforts on generalizing RPA based on equation of motion, adiabatic connections, or ring approximation of multi-reference coupled cluster theories[31–44], our MR-RPA formulation has a distinct feature that it is derived from a clear diagrammatic resummation following the spirit of its single-reference counterpart by Gell-Mann and Brueckner[8]. Therefore, it is systematically improvable by simply adding more diagrams as illustrated by MR-SOSEX. The present generalized MBPT framework successfully bridges two fields – MBPT in condensed matter physics[1–3, 5, 45] and multi-reference perturbation theory (MRPT) in quantum chemistry[46], and constitutes an important fundamental step towards developing accurate simulation methods via diagrammatic resummation.

Generalized many-body perturbation theory.— To solve the electronic Schrödinger equation $\hat{H}|\Psi\rangle = E|\Psi\rangle$ using perturbation theory, we first introduce a partition of the

second-quantized electronic Hamiltonian \hat{H} , viz.,

$$\hat{H} = \hat{H}_0 + \hat{V}, \quad (1)$$

$$\hat{H}_0 = h_{pq}\hat{p}^\dagger\hat{q} + \frac{1}{2}h_{pr,qs}\hat{p}^\dagger\hat{q}^\dagger\hat{s}\hat{r}, \quad (2)$$

$$\hat{V} = v_{pq}\hat{p}^\dagger\hat{q} + \frac{1}{2}v_{pr,qs}\hat{p}^\dagger\hat{q}^\dagger\hat{s}\hat{r}, \quad (3)$$

where the Einstein summation convention for repeated indices has been implied, h_{pq} ($h_{pr,qs}$) and v_{pq} ($v_{pr,qs}$) are the zeroth-order and first-order one-electron (two-electron) interactions, respectively, and $\hat{p}^{(\dagger)}$ represents the Fermionic annihilation (creation) operator for the p -th spin-orbital. The sum of $h_{pr,qs}$ and $v_{pr,qs}$ obeys $h_{pr,qs} + v_{pr,qs} = \langle pq|rs\rangle$, where $\langle pq|rs\rangle$ denotes the two-electron Coulomb integral[1, 3]. Standard MBPT corresponds to $h_{pr,qs} \equiv 0$, resulting in a quadratic \hat{H}_0 whose eigenstates are Slater determinants. Here, we relax this restriction, allowing certain parts of $h_{pr,qs}$ corresponding to strong electron interactions nonzero. This implies that the eigenfunction of \hat{H}_0 will be a multi-determinant wavefunction in general, and the Wick's theorem[47] does not hold. The specific choice of \hat{H}_0 will be discussed later.

We assume that $|\Phi_0\rangle$ ($|\Psi_0\rangle$) and $E_0^{(0)}$ (E_0) are the non-degenerate ground-state wavefunction and energy of \hat{H}_0 (\hat{H}), respectively. Then, the energy correction $\Delta E = E_0 - E_0^{(0)}$ can be expressed by[5] (see Supplementary Material[48])

$$\Delta E = \lim_{T \rightarrow \infty} \frac{i}{T} \ln \langle \hat{U}(\frac{T}{2}, -\frac{T}{2}) \rangle_0, \quad (4)$$

where $\langle \hat{U}(\frac{T}{2}, -\frac{T}{2}) \rangle_0$ is a shorthand notation for $\langle \Phi_0 | \hat{U}(\frac{T}{2}, -\frac{T}{2}) | \Phi_0 \rangle$, $\hat{U}(\frac{T}{2}, -\frac{T}{2}) = \mathcal{T} \exp\left(-i \int_{-\frac{T}{2}}^{\frac{T}{2}} \hat{V}(t) dt\right)$ with $\hat{V}(t) = e^{i\hat{H}_0 t} \hat{V} e^{-i\hat{H}_0 t}$, and \mathcal{T} is the time-ordering operator. Throughout this work, the time variable t will be understood to be on a contour[5] $\mathcal{C} = \{t \equiv (1 - i\eta)\tilde{t} : \tilde{t} \in \mathbb{R}, \eta > 0\}$ with η being an infinitesimal parameter, and the factor $-i\eta$ will only be explicitly included when necessary. Introducing an order counting parameter λ for \hat{V} in Eq. (1), we can express $\langle \hat{U}(\frac{T}{2}, -\frac{T}{2}) \rangle_0 = \sum_{n=0}^{\infty} \frac{\lambda^n}{n!} \mu_n$ where

$$\mu_n = (-i)^n \int_{-\frac{T}{2}}^{\frac{T}{2}} dt_1 \cdots \int_{-\frac{T}{2}}^{\frac{T}{2}} dt_n \langle \mathcal{T}[\hat{V}(t_1) \cdots \hat{V}(t_n)] \rangle_0. \quad (5)$$

The use of cumulant decomposition[5, 49] for the time-ordered Green's functions encountered in Eq. (5) will lead to a generalization of the Feynman diagrams in standard MBPT.

To illustrate this, we consider the second-order energy correction ΔE_2 due to one-body perturbations for simplicity. The integrand for ΔE_2 in this case involves $v_{pr}v_{qs} \langle \mathcal{T}[\hat{p}^\dagger(t_1^\dagger)\hat{r}(t_1)\hat{q}^\dagger(t_2^\dagger)\hat{s}(t_2)] \rangle_0 - \langle \hat{p}^\dagger\hat{r} \rangle_0 \langle \hat{q}^\dagger\hat{s} \rangle_0$. We can identify $\langle \mathcal{T}[\hat{p}^\dagger(t_1^\dagger)\hat{r}(t_1)\hat{q}^\dagger(t_2^\dagger)\hat{s}(t_2)] \rangle_0$ as the zeroth-order two-body Green's function $-G_{rs,pq}^0(t_1, t_2, t_1^\dagger, t_2^\dagger)$,

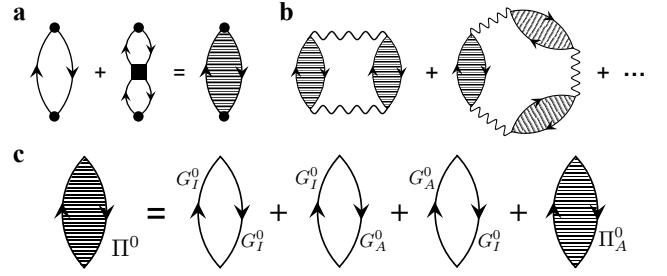


FIG. 1. Generalized diagrammatic expansion. (a) Illustration of the second-order energy due to one-body perturbations (black dot). Each directed line connecting two interactions in the first diagram is a one-body Green's function G_{pq}^0 . The black square along with two incoming and outgoing lines in the second diagram represent a connected two-body Green's function $G_{rs,pq}^{0,c}$ in Eq. (6). The sum of the two diagrams (without considering interactions) forms the polarizability $\Pi_{pr,qs}^0$ (black bubble) in Eq. (8). (b) Definition of MR-RPA correlation energy in terms of a summation of generalized ring diagrams, where the polarizabilities defined in (a) are connected by the residual interaction (wiggly lines) $v_{pr,qs}$ in Eq. (3). (c) Using the CASSCF reference and the Dyall Hamiltonian \hat{H}_D in Eq. (18), the polarizability can be separated into four parts, where G_I^0 and G_A^0 are the Green's functions for inactive and active orbitals, respectively, and only the part solely involving active orbitals contains a non-vanishing contribution from $G_{rs,pq}^{0,c}$.

and express it in terms of connected Green's functions[5, 49]

$$\begin{aligned} & G_{rs,pq}^0(t_1, t_2, t_1^\dagger, t_2^\dagger) \\ &= G_{rp}^0(t_1, t_1^\dagger)G_{sq}^0(t_2, t_2^\dagger) - G_{rq}^0(t_1, t_2^\dagger)G_{sp}^0(t_2, t_1^\dagger) \\ & \quad + G_{rs,pq}^{0,c}(t_1, t_2, t_1^\dagger, t_2^\dagger), \end{aligned} \quad (6)$$

where $G_{pq}^0(t_1, t_2) = -i \langle \mathcal{T}[\hat{p}(t_1)\hat{q}^\dagger(t_2)] \rangle_0$ is the zeroth-order one-body Green's function and $G_{rs,pq}^{0,c}$ represents the connected component of $G_{rs,pq}^0$, which is nonzero for a generic \hat{H}_0 (2). Then, the integrand becomes $v_{pr}v_{qs} (-G_{rs,pq}^0(t_1, t_2, t_1^\dagger, t_2^\dagger) + G_{rp}^0(t_1, t_1^\dagger)G_{sq}^0(t_2, t_2^\dagger)) = v_{pr}v_{qs} (G_{rq}^0(t_1, t_2^\dagger)G_{sp}^0(t_2, t_1^\dagger) - G_{rs,pq}^{0,c}(t_1, t_2, t_1^\dagger, t_2^\dagger))$, which can be represented by two connected diagrams, see Fig. 1(a). Similar construction can be generalized to arbitrary order for the partition (1). Consequently, analogous to the single-reference linked cluster theorem[50], we can rewrite Eq. (4) as

$$\begin{aligned} \Delta E_n &= \lim_{T \rightarrow \infty} \frac{i}{T} \frac{(-i)^n}{n!} \int_{-\frac{T}{2}}^{\frac{T}{2}} dt_1 \cdots \int_{-\frac{T}{2}}^{\frac{T}{2}} dt_n \\ & \quad \langle \mathcal{T}[\hat{V}(t_1) \cdots \hat{V}(t_n)] \rangle_{0, \text{linked}}, \end{aligned} \quad (7)$$

where the subscript 'linked' refers to linked diagrams, which in this case not only include both standard Feynman diagrams (composed of interactions and G_{pq}^0), but also new diagrams involving connected zeroth-order many-body Green's functions. In the special case that

\hat{H}_0 is quadratic and $|\Phi_0\rangle$ is a Slater determinant, all connected many-body Green's functions vanish due to Wick's theorem[47] such that the present diagrammatic expansion reduces to standard MBPT using Feynman diagrams[50].

Multi-reference random phase approximation.— In the language of Feynman diagrams, the traditional single-reference RPA (SR-RPA) amounts to a resummation of ring diagrams to infinite order[7, 8]. In terms of the generalized diagrams described above, we can extend SR-RPA to the multi-reference case by defining MR-RPA as a summation of the generalized ring diagrams, see Fig. 1(b), where two interactions can be connected either by the conventional product of two Green's functions $G_{rq}(t_1, t_2^+)G_{sp}(t_2, t_1^+)$ or by a connected two-body Green's function $G_{rs,pq}^{0,c}(t_1, t_2, t_1^+, t_2^+)$. Thus, the local structure of the generalized ring diagrams is exactly the same as that in Fig. 1(a) discussed before. We can rewrite the sum of these two contributions

$$\begin{aligned} & G_{rq}^0(t_1, t_2^+)G_{sp}^0(t_2, t_1^+) - G_{rs,pq}^{0,c}(t_1, t_2, t_1^+, t_2^+) \\ &= \langle \mathcal{T} [(\hat{p}^\dagger(t_1^+)\hat{r}(t_1) - \langle \hat{p}^\dagger \hat{r} \rangle_0)(\hat{q}^\dagger(t_2^+)\hat{s}(t_2) - \langle \hat{q}^\dagger \hat{s} \rangle_0)] \rangle_0 \\ &\equiv i\Pi_{pr,qs}^0(t_1, t_2), \end{aligned} \quad (8)$$

in terms of the irreducible polarizability[45] (polarization propagator) $\Pi_{pr,qs}^0(t_1, t_2)$. Then, the MR-RPA correlation energy defined in Fig. 1(b) can be found as (see Supplementary Material[48])

$$\Delta E^{\text{RPA}} = \int_{-\infty}^{+\infty} \frac{d\omega}{2\pi} \frac{1}{2} \text{tr} [\ln[\mathbf{I} - \mathbf{v}\Pi^0(i\omega)] + \mathbf{v}\Pi^0(i\omega)] \quad (9)$$

with $v_{pr,qs}$ given in Eq. (3). This expression is exactly the same as that for SR-RPA[10, 14, 51]. Thus, our MR-RPA can be viewed as a natural generalization of SR-RPA to more general two-electron perturbation and irreducible polarizability.

Dyson equation and plasmon formula.— To gain a deeper insight into the obtained MR-RPA, we introduce a reducible polarizability in the form of a Dyson equation

$$\mathbf{\Pi}^\lambda(z) = \mathbf{\Pi}^0(z) + \lambda \mathbf{\Pi}^0(z) \mathbf{v} \mathbf{\Pi}^\lambda(z), \quad (10)$$

where z is a complex frequency and λ is the order parameter associated with \hat{V} . Then, Eq. (9) can be rewritten as a coupling constant integration

$$\Delta E^{\text{RPA}} = -\frac{1}{2} \int_0^1 d\lambda \int_{-\infty}^{\infty} \frac{d\omega}{2\pi} \text{tr}(\mathbf{v}[\mathbf{\Pi}^\lambda(i\omega) - \mathbf{\Pi}^0(i\omega)]). \quad (11)$$

Using the spectral representation of $\Pi_{pr,qs}^0(z) = \sum_{N>0} \left[\frac{\langle 0|\hat{p}^\dagger \hat{r}|N\rangle \langle N|\hat{q}^\dagger \hat{s}|0\rangle}{z - \omega_N} - \frac{\langle 0|\hat{q}^\dagger \hat{s}|N\rangle \langle N|\hat{p}^\dagger \hat{r}|0\rangle}{z + \omega_N} \right]$, where the ground and excited states of \hat{H}_0 are abbreviated by $|0\rangle$ and $|N\rangle$, respectively, and $\omega_N = E_N^{(0)} - E_0^{(0)}$ is the zeroth-order excitation energy, both integrations in Eq.

(11) can be performed analytically (see Supplementary Material[48]), such that

$$\Delta E^{\text{RPA}} = \frac{1}{2} \sum_{I>0} (\Omega_I^{\text{RPA}} - \Omega_I^{\text{TDA}}), \quad (12)$$

where $I > 0$ means that only positive Ω is concerned. Eq. (12) is usually referred to as the plasmon formula in SR-RPA[14]. Here, we generalize it to the multi-reference case, with Ω_I^{RPA} given by the following MR-RPA eigenvalue problem

$$\begin{bmatrix} \mathbf{A} & \mathbf{B} \\ \mathbf{B}^* & \mathbf{A}^* \end{bmatrix} \begin{bmatrix} \mathbf{x}_I \\ \mathbf{y}_I \end{bmatrix} = \begin{bmatrix} \mathbf{I} & \mathbf{0} \\ \mathbf{0} & -\mathbf{I} \end{bmatrix} \begin{bmatrix} \mathbf{x}_I \\ \mathbf{y}_I \end{bmatrix} \Omega_I, \quad (13)$$

where matrices \mathbf{A} ($= \mathbf{A}^\dagger$) and \mathbf{B} ($= \mathbf{B}^T$) are defined by

$$A_{NM} = \omega_N \delta_{NM} + \langle N|\hat{p}^\dagger \hat{r}|0\rangle v_{pr,qs} \langle 0|\hat{q}^\dagger \hat{s}|M\rangle, \quad (14)$$

$$B_{NM} = \langle N|\hat{p}^\dagger \hat{r}|0\rangle v_{pr,qs} \langle M|\hat{q}^\dagger \hat{s}|0\rangle, \quad (15)$$

respectively, with $N, M > 0$ labeling excited states of \hat{H}_0 and the Einstein summation convention assumed for repeated orbital indices. Ω_I^{TDA} corresponds to the eigenvalue of Eq. (13) with \mathbf{B} set to zero, which is often called the Tamm-Dancoff approximation (TDA) in SR-RPA[52, 53]. When \hat{H}_0 is quadratic, Eq. (13) reduces to the SR-RPA equation, since $\langle N|\hat{p}^\dagger \hat{r}|0\rangle$ is nonzero only if $|N\rangle = \hat{p}^\dagger \hat{r}|0\rangle$ with r and p referring to occupied and virtual orbitals, respectively.

Multi-reference second-order screened exchange correction.— So far, MR-RPA is developed without considering exchange, and hence it will suffer from self-interaction error (SIE) as SR-RPA[29, 54, 55]. A simple way to include exchange is to generalize the second-order screened exchange (SOSEX) correction[18] to the multi-reference case. Specifically, the connection between Eq. (13) for SR-RPA and the direct ring coupled cluster doubles (drCCD) equation

$$\mathbf{B}^* + \mathbf{A}^* \mathbf{T} + \mathbf{T} \mathbf{A} + \mathbf{T} \mathbf{B} \mathbf{T} = \mathbf{0}, \quad (16)$$

has been established[23], where $\mathbf{T} = \mathbf{Y} \mathbf{X}^{-1}$ with \mathbf{X} and \mathbf{Y} being the eigenvectors of Eq. (13) with positive eigenvalues. The SR-SOSEX[18] amounts to evaluate Eq. (12) by using its equivalent form

$$\Delta E^{\text{RPA}} = \frac{1}{2} \text{tr}(\mathbf{B} \mathbf{T}), \quad (17)$$

but with $v_{pr,qs}$ in \mathbf{B} replaced by its antisymmetrized counterpart $v_{pr,qs} - v_{ps,qr}$. Since our MR-RPA equation has exactly the same mathematical form, the similar derivation leads naturally to MR-SOSEX (see Supplementary Material[48] for details).

Choice of zeroth-order Hamiltonian.— The above MR-RPA and MR-SOSEX are general in the sense that they can be applied to any partition of form (1). However, to be both computationally feasible and accurate,

the choice of zeroth-order Hamiltonian is crucial. In this work, we employ the complete active space self-consistent field[3] (CASSCF) wavefunction as the zeroth-order state, which is the usual starting point of multi-reference perturbation theory in quantum chemistry[46], and the Dyall Hamiltonian[56] as \hat{H}_0 among other possible partitions[57, 58]. The Dyall Hamiltonian \hat{H}_D contains two parts (see Supplementary Material[48] for detailed definitions of ϵ_i , ϵ_a and f_{xy})

$$\hat{H}_D = \hat{H}_I + \hat{H}_A, \quad (18)$$

$$\hat{H}_I = \epsilon_i \hat{i}^\dagger \hat{i} + \epsilon_a \hat{a}^\dagger \hat{a}, \quad (19)$$

$$\hat{H}_A = f_{xy} \hat{x}^\dagger \hat{y} + \frac{1}{2} \langle xy|zw \rangle \hat{x}^\dagger \hat{y}^\dagger \hat{w} \hat{z}, \quad (20)$$

where the so-called inactive part \hat{H}_I is quadratic for the doubly occupied and virtual orbitals, while the active part \hat{H}_A retains the full two-electron Coulomb interactions among the M_A active orbitals, within which the electron correlation is supposed to be stronger. Due to its additive separability, all of its eigenfunctions (e.g., the CASSCF ground state $|0\rangle = |\Theta_0\rangle |\Phi_0^{N_A}\rangle$) are products of an inactive part ($|\Theta_0\rangle$), which is simply a Slater determinant, and an active part ($|\Phi_0^{N_A}\rangle$), which is a multi-determinant wavefunction that describes the strong correlation among the N_A active electrons within the active space denoted by $\text{CAS}(N_A, M_A)$. Consequently, the zeroth-order excited state $|N\rangle$ ($N > 0$) that can couple with $|0\rangle$ in Eqs. (14) and (15) must belong to the following four classes of excitations (see Fig. S2 in the Supplemental Material[48])

$$\{|\Theta_i^a\rangle |\Phi_0^{N_A}\rangle, |\Theta_i\rangle |\Phi_\mu^{N_A+1}\rangle, |\Theta^a\rangle |\Phi_\mu^{N_A-1}\rangle, |\Theta_0\rangle |\Phi_{\mu>0}^{N_A}\rangle\}, \quad (21)$$

where $|\Theta_i^a\rangle = \hat{a}^\dagger \hat{i} |\Theta_0\rangle$, $|\Theta_i\rangle = \hat{i} |\Theta_0\rangle$, $|\Theta^a\rangle = \hat{a}^\dagger |\Theta_0\rangle$, and $|\Phi_\mu^{N_A}\rangle$ represents the μ -th eigenstate of \hat{H}_A with N_A electrons. The first class is similar to that in SR-RPA, while the latter three classes are excitations involving the active orbitals, which can be multiple-electron excitations in nature. In particular, the fourth class describes excitations within the active space. All of them contribute to the screening of two-electron interactions at the MR-RPA level, see Fig. 1(c), which goes beyond the conventional SR-RPA screening by particle-hole excitations only. Detailed matrix elements of the resulting 4-by-4 block matrices (**A** and **B**) are presented in Supplementary Material[48].

Results.— We implemented MR-RPA and MR-SOSEX using the PySCF package[59] (see Supplementary Material[48] for details), and compare their performances with their single-reference counterparts for prototypical molecules. Figure 2 shows the potential energy curves (PECs) computed by various SR and MR methods using the cc-pVDZ basis set[60] for H_2^+ and H_2 , which have become the testbed for RPA[20, 28, 55]. It

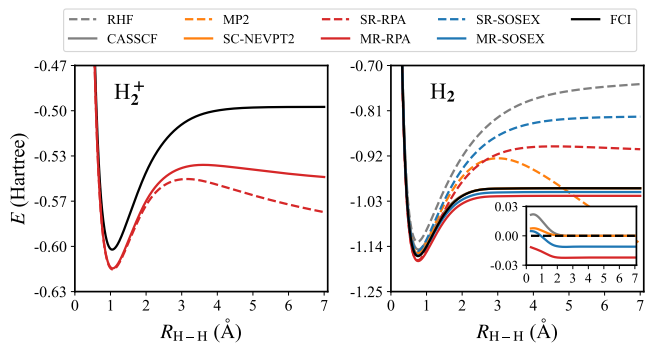


FIG. 2. Bond dissociation of H_2^+ and H_2 calculated by different methods using the cc-pVDZ basis set. The active spaces used for H_2^+ and H_2 are CAS(1,1) and CAS(2,2), respectively. For H_2^+ , other methods including RHF, MP2, CASSCF, SR-SOSEX, and MR-SOSEX are all exact, and hence not displayed for clarity. The inset in the right figure shows the errors of multi-reference results with respect to the FCI result.

is seen that for H_2^+ , both SR-RPA and MR-RPA suffer from SIE due to the lack of exchange, while SR-SOSEX and MR-SOSEX are exact. The SIE in MR-RPA is smaller, because the two-electron interactions in \hat{H}_A (20) are treated exactly with exchange included. For H_2 , as the bond distance increases, the PEC computed by the second order Møller-Plesset perturbation (MP2) starting from restricted Hartree-Fock (RHF) reference diverges, and both SR-RPA and SR-SOSEX fail. Compared against the exact full configuration interaction (FCI) reference, the improvements by MR-RPA and MR-SOSEX are dramatic. The non-parallel errors (NPEs) of MR-RPA and MR-SOSEX are 8.79 and 13.30 milli-Hartree (mH), respectively, which are much smaller than the NPE of CASSCF (18.27 mH) and are slightly larger than that (6.44 mH) of a widely used second-order MRPT – the strongly contracted second-order n -electron valence perturbation theory (SC-NEVPT2)[61].

Figure 3 displays the bond dissociation of four typical molecules - HF, ScH, H_2O , and N_2 (see Supplementary Material[48] for detailed results). As demonstrated by the occupation numbers of the CASSCF natural orbitals (NO) within the active space, the electron correlation is progressively stronger from HF to N_2 . Again, we found that both SR-RPA and SR-SOSEX fail miserably at stretched geometries, indicating the break down of standard MBPT based on a RHF reference. At short bond distance (ca. $<1\text{\AA}$), where electron correlation is weak and the RHF and CASSCF energies are close to each other, our MR generalizations are consistent with their SR counterparts. However, at larger bond distance, MR-RPA and MR-SOSEX improve their SR counterparts significantly by treating strong correlation among active orbitals at the zeroth order. This is particularly important for N_2 , where the SR-RPA/SOSEX

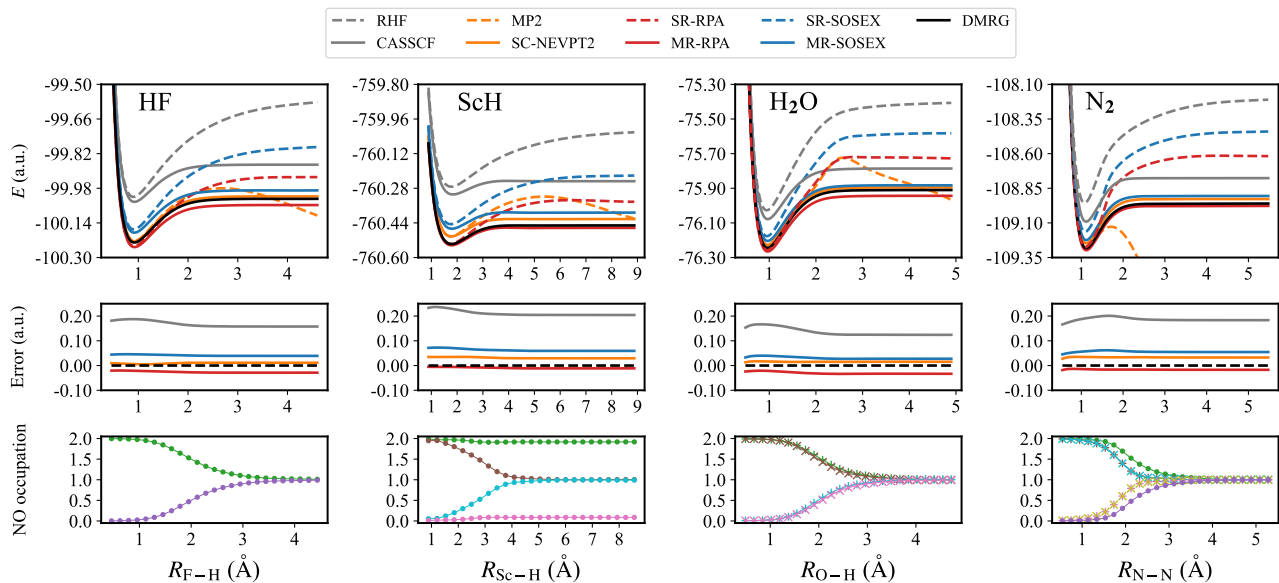


FIG. 3. Potential energy curves for four molecules (HF, ScH, H₂O and N₂) computed with different methods using the cc-pVDZ basis set. Errors of multi-reference results with respect to the nearly exact DMRG results are shown in the middle. The active spaces are CAS(2,2), CAS(4,4), CAS(4,4), and CAS(6,6) for HF, ScH, H₂O and N₂, respectively, with the CASSCF natural orbital (NO) occupation numbers shown below. Significant deviations from 0 or 2 indicate the presence of strong electron correlation.

curves deviate considerably from the corresponding MR-RPA/SOSEX results already around the equilibrium geometry. Note that since CASSCF completely misses the weak dynamic correlation, the CASSCF PECs are much higher than the nearly exact results obtained by using the *ab initio* density matrix renormalization group (DMRG) algorithm[62–64]. In contrast, MR-RPA and MR-SOSEX treat both strong and weak electron correlation in a more balanced way, and hence lead to a good agreement with the DMRG results for realistic molecules. As shown in Fig. 3, the performances of MR-RPA, MR-SOSEX, and SC-NEVPT2 are comparable. All of them significantly improve CASSCF for dissociation energies and NPEs (see Table S7 in Supplementary Material).

Conclusion.— We developed a generalized MBPT starting from an interacting \hat{H}_0 and formulated a multi-reference generalization of RPA and SOSEX using diagrammatic resummation within this framework. Compared with other multi-reference generalizations of RPA[31–44], our diagrammatic approach leads to a more natural generalization in the sense that it gives rise to a set of unified equations that work in both SR and MR cases. As demonstrated for bond dissociation of molecules, MR-RPA/SOSEX show significant improvements over traditional SR-RPA/SOSEX in the presence of strong correlation. This work opens up new possibilities for advancing *ab initio* computational methods for strongly correlated systems via diagrammatic resummations. Promising directions include the development of low-scaling algorithms for large molecules [65–67] and the

combination with density functional theory for materials.

Acknowledgments.— The authors acknowledge Yang Guo and Xinguo Ren for helpful comments on the manuscript. This work was supported by the Innovation Program for Quantum Science and Technology (Grant No. 2023ZD0300200) and the Fundamental Research Funds for the Central Universities.

* zhendongli@bnu.edu.cn

- [1] R. M. Martin, L. Reining, and D. M. Ceperley, *Interacting electrons* (Cambridge University Press, 2016).
- [2] P. Coleman, *Introduction to Many-Body Physics* (Cambridge University Press, 2015).
- [3] T. Helgaker, P. Jørgensen, and J. Olsen, *Molecular electronic-structure theory* (John Wiley & Sons, 2013).
- [4] A. Fetter and J. Walecka, *Quantum Theory of Many-Particle System*, International Series in Pure and Applied Physics (MacGraw-Hill, New York, 1971).
- [5] J. W. Negele and H. Orland, *Quantum Many-particle Systems* (CRC Press, Boca Raton, 1998).
- [6] D. Pines and D. Bohm, Phys. Rev. **85**, 338 (1952).
- [7] D. Bohm and D. Pines, Phys. Rev. **92**, 609 (1953).
- [8] M. Gell-Mann and K. A. Brueckner, Phys. Rev. **106**, 364 (1957).
- [9] A. Hesselmann and A. Görling, Mol. Phys. **109**, 2473 (2011).
- [10] X. Ren, P. Rinke, C. Joas, and M. Scheffler, J. Mater. Sci. **47**, 7447 (2012).
- [11] H. Eshuis, J. E. Bates, and F. Furche, Theor. Chem. Acc. **131**, 1084 (2012).

- [12] G. P. Chen, V. K. Voora, M. M. Agee, S. G. Balasubramani, and F. Furche, *Annu. Rev. Phys. Chem.* **68**, 421 (2017).
- [13] D. C. Langreth and J. P. Perdew, *Phys. Rev. B* **15**, 2884 (1977).
- [14] F. Furche, *J. Chem. Phys.* **129**, 114105 (2008).
- [15] J. Toulouse, I. C. Gerber, G. Jansen, A. Savin, and J. G. Ángyán, *Phys. Rev. Lett.* **102**, 096404 (2009).
- [16] J. Paier, B. G. Janesko, T. M. Henderson, G. E. Scuseria, A. Grüneis, and G. Kresse, *J. Chem. Phys.* **132**, 094103 (2010).
- [17] A. Heßelmann and A. Görling, *Phys. Rev. Lett.* **106**, 093001 (2011).
- [18] A. Grüneis, M. Marsman, J. Harl, L. Schimka, and G. Kresse, *J. Chem. Phys.* **131**, 154115 (2009).
- [19] J. G. Ángyán, R.-F. Liu, J. Toulouse, and G. Jansen, *J. Chem. Theory Comput.* **7**, 3116 (2011).
- [20] J. E. Bates and F. Furche, *J. Chem. Phys.* **139**, 171103 (2013).
- [21] F. Hummel, A. Grüneis, G. Kresse, and P. Ziesche, *J. Chem. Theory Comput.* **15**, 3223 (2019).
- [22] X. Ren, A. Tkatchenko, P. Rinke, and M. Scheffler, *Phys. Rev. Lett.* **106**, 153003 (2011).
- [23] G. E. Scuseria, T. M. Henderson, and D. C. Sorensen, *J. Chem. Phys.* **129**, 231101 (2008).
- [24] G. Jansen, R.-F. Liu, and J. G. Ángyán, *J. Chem. Phys.* **133**, 154106 (2010).
- [25] D. Peng, S. N. Steinmann, H. van Aggelen, and W. Yang, *J. Chem. Phys.* **139**, 104112 (2013).
- [26] G. E. Scuseria, T. M. Henderson, and I. W. Bulik, *J. Chem. Phys.* **139**, 104113 (2013).
- [27] H. van Aggelen, Y. Yang, and W. Yang, *Phys. Rev. A* **88**, 030501 (2013).
- [28] H. van Aggelen, Y. Yang, and W. Yang, *J. Chem. Phys.* **140**, 18A511 (2014).
- [29] M. N. Tahir and X. Ren, *Phys. Rev. B* **99**, 195149 (2019).
- [30] A. Ammar, A. Marie, M. Rodríguez-Mayorga, H. G. Burton, and P.-F. Loos, *J. Chem. Phys.* **160** (2024).
- [31] D. L. Yeager and P. Jørgensen, *Chem. Phys. Lett.* **65**, 77 (1979).
- [32] P. Jørgensen, H. J. A. Jensen, and J. Olsen, *J. Chem. Phys.* **89**, 3654 (1988).
- [33] B. Helmich-Paris, *J. Chem. Phys.* **150**, 174121 (2019).
- [34] K. Chatterjee and K. Pernal, *J. Chem. Phys.* **137**, 204109 (2012).
- [35] K. Pernal, *J. Chem. Theory Comput.* **10**, 4332 (2014).
- [36] K. Chatterjee, E. Pastorczak, K. Jawulski, and K. Pernal, *J. Chem. Phys.* **144**, 244111 (2016).
- [37] K. Pernal, *Phys. Rev. Lett.* **120**, 013001 (2018).
- [38] K. Pernal, *J. Chem. Phys.* **149**, 204101 (2018).
- [39] E. Pastorczak and K. Pernal, *J. Chem. Theory Comput.* **14**, 3493 (2018).
- [40] D. Drwal, P. Beran, M. Hapka, M. Modrzejewski, A. Sokół, L. Veis, and K. Pernal, *J. Phys. Chem. Lett.* **13**, 4570 (2022).
- [41] M. Matoušek, M. Hapka, L. Veis, and K. Pernal, *J. Chem. Phys.* **158**, 054105 (2023).
- [42] Y. Guo and K. Pernal, *Faraday Discuss.* (2024), 10.1039/D4FD00054D.
- [43] Á. Szabados and Á. Margócsy, *Mol. Phys.* **115**, 2731 (2017).
- [44] Á. Margócsy and Á. Szabados, *J. Chem. Phys.* **152**, 204114 (2020).
- [45] G. Stefanucci and R. Van Leeuwen, *Nonequilibrium many-body theory of quantum systems: a modern introduction* (Cambridge University Press, 2013).
- [46] J. W. Park, R. Al-Saadon, M. K. MacLeod, T. Shiozaki, and B. Vlaisavljevich, *Chem. Rev.* **120**, 5878 (2020).
- [47] G.-C. Wick, *Phys. Rev.* **80**, 268 (1950).
- [48] See Supplemental Material at URL-will-be-inserted-by-publisher for details of derivations for MR-RPA, implementations and numerical results.
- [49] W. Metzner, *Phys. Rev. B* **43**, 8549 (1991).
- [50] J. Goldstone, *Proc. R. Soc. A* **239**, 267 (1957).
- [51] A. Heßelmann, *Phys. Rev. A* **85**, 012517 (2012).
- [52] I. Tamm, *J. Phys. (USSR)* **9**, 449 (1945).
- [53] S. M. Dancoff, *Phys. Rev.* **78**, 382 (1950).
- [54] T. M. Henderson and G. E. Scuseria, *Mol. Phys.* **108**, 2511 (2010).
- [55] P. Mori-Sánchez, A. J. Cohen, and W. Yang, *Phys. Rev. A* **85**, 042507 (2012).
- [56] K. G. Dyall, *J. Chem. Phys.* **102**, 4909 (1995).
- [57] E. Rosta and P. R. Surján, *J. Chem. Phys.* **116**, 878 (2002).
- [58] R. F. Fink, *Chem. Phys.* **356**, 39 (2009).
- [59] Q. Sun, X. Zhang, S. Banerjee, P. Bao, M. Barbry, N. S. Blunt, N. A. Bogdanov, G. H. Booth, J. Chen, Z.-H. Cui, J. J. Eriksen, Y. Gao, S. Guo, J. Hermann, M. R. Hermes, K. Koh, P. Koval, S. Lehtola, Z. Li, J. Liu, N. Mardirossian, J. D. McClain, M. Motta, B. Mussard, H. Q. Pham, A. Pulkin, W. Purwanto, P. J. Robinson, E. Ronca, E. R. Sayfutyarova, M. Scheurer, H. F. Schurkus, J. E. T. Smith, C. Sun, S.-N. Sun, S. Upadhyay, L. K. Wagner, X. Wang, A. White, J. D. Whitfield, M. J. Williamson, S. Wouters, J. Yang, J. M. Yu, T. Zhu, T. C. Berkelbach, S. Sharma, A. Y. Sokolov, and G. K.-L. Chan, *J. Chem. Phys.* **153**, 024109 (2020).
- [60] T. H. Dunning, Jr., *J. Chem. Phys.* **90**, 1007 (1989).
- [61] C. Angeli, R. Cimiraglia, S. Evangelisti, T. Leininger, and J.-P. Malrieu, *J. Chem. Phys.* **114**, 10252 (2001).
- [62] S. R. White, *Phys. Rev. Lett.* **69**, 2863 (1992).
- [63] G. K.-L. Chan and S. Sharma, *Annu. Rev. Phys. Chem.* **62**, 465 (2011).
- [64] C. Xiang, W. Jia, W.-H. Fang, and Z. Li, *J. Chem. Theory Comput.* **20**, 775 (2024).
- [65] H. Eshuis, J. Yarkony, and F. Furche, *J. Chem. Phys.* **132** (2010).
- [66] X. Ren, P. Rinke, V. Blum, J. Wiefierink, A. Tkatchenko, A. Sanfilippo, K. Reuter, and M. Scheffler, *New J. Phys.* **14**, 053020 (2012).
- [67] M. Kaltak, J. Klimeš, and G. Kresse, *Phys. Rev. B* **90**, 054115 (2014).
- [68] I. Shavitt and R. J. Bartlett, *Many-body methods in chemistry and physics: MBPT and coupled-cluster theory* (Cambridge university press, 2009).
- [69] Z. Li, *J. Chem. Phys.* **151**, 244114 (2019).

Supplemental material for “Generalized many-body perturbation theory for the electron correlation energy”

Yuqi Wang, Wei-Hai Fang, and Zhendong Li

CONTENTS

S1. Details of derivations for MR-RPA	1
A. Proof of the energy correction formula - Eq. (4)	1
B. Proof of the MR-RPA correlation energy - Eq. (9)	2
C. Proof of the plasmon formula - Eq. (12)	4
D. Connection to coupled-cluster theory	6
S2. Matrix elements of MR-RPA with a CASSCF reference	7
S3. Computational details and numerical results	9
A. Computational details	9
B. SR-RPA implemented for comparison	9
C. Results for H_2^+ , H_2 , HF, ScH, H_2O , and N_2	9

S1. DETAILS OF DERIVATIONS FOR MR-RPA

A. Proof of the energy correction formula - Eq. (4)

The proof of the energy correction formula (4) largely follows from Ref. [5]. We start from a partition of the time-independent Hamiltonian as

$$\hat{H} = \hat{H}_0 + \hat{V}. \quad (\text{S1})$$

The eigenvalues and eigenvectors of \hat{H}_0 and \hat{H} are defined by

$$\hat{H}_0|\Phi_n\rangle = E_n^{(0)}|\Phi_n\rangle, \quad (\text{S2})$$

$$\hat{H}|\Psi_n\rangle = E_n|\Psi_n\rangle. \quad (\text{S3})$$

The time-evolution operator under the interaction picture can be written explicitly as

$$\hat{U}(t, t_0) = e^{i\hat{H}_0 t} e^{-i\hat{H}(t-t_0)} e^{-i\hat{H}_0 t_0}. \quad (\text{S4})$$

Let $t = \frac{T}{2}$ and $t_0 = -\frac{T}{2}$, it becomes

$$\hat{U}\left(\frac{T}{2}, -\frac{T}{2}\right) = e^{i\hat{H}_0 T/2} e^{-i\hat{H}T} e^{i\hat{H}_0 T/2}, \quad (\text{S5})$$

such that the expectation value of $|\Phi_0\rangle$ is

$$\langle \hat{U}\left(\frac{T}{2}, -\frac{T}{2}\right) \rangle_0 = e^{iE_0^{(0)}T} \langle e^{-i\hat{H}T} \rangle_0. \quad (\text{S6})$$

Using the resolution of identity (RI) $\sum_n |\Psi_n\rangle\langle\Psi_n| = \hat{1}$, we get

$$\begin{aligned} \langle \hat{U}\left(\frac{T}{2}, -\frac{T}{2}\right) \rangle_0 &= e^{iE_0^{(0)}T} \sum_n \langle \Phi_0 | e^{-i\hat{H}T} | \Psi_n \rangle \langle \Psi_n | \Phi_0 \rangle \\ &= e^{iE_0^{(0)}T} \sum_n |\langle \Phi_0 | \Psi_n \rangle|^2 e^{-iE_n T} \\ &= e^{-i\Delta E T} \left(|\langle \Phi_0 | \Psi_0 \rangle|^2 + \sum_{n \geq 1} |\langle \Phi_0 | \Psi_n \rangle|^2 e^{-i(E_n - E_0)T} \right), \end{aligned} \quad (\text{S7})$$

where $\Delta E \equiv E_0 - E_0^{(0)}$. Take the logarithm on both sides,

$$\frac{i}{T} \ln \langle \hat{U}(\frac{T}{2}, -\frac{T}{2}) \rangle_0 = \Delta E + \frac{i}{T} \ln \left(|\langle \Phi_0 | \Psi_0 \rangle|^2 + \sum_{n \geq 1} |\langle \Phi_0 | \Psi_n \rangle|^2 e^{-i(E_n - E_0)T} \right). \quad (\text{S8})$$

Now considering T on the contour[5] $\mathcal{C} = \{t \equiv (1 - i\eta)\tilde{t} : \tilde{t} \in \mathbb{R}, \eta > 0\}$, Eq. (S8) becomes

$$\frac{i}{T - i\eta} \ln \langle \hat{U}(\frac{T - i\eta}{2}, -\frac{T - i\eta}{2}) \rangle_0 = \Delta E + \frac{i}{T - i\eta} \ln \left(|\langle \Phi_0 | \Psi_0 \rangle|^2 + \sum_{n \geq 1} |\langle \Phi_0 | \Psi_n \rangle|^2 e^{-i(E_n - E_0)T} e^{-(E_n - E_0)\eta T} \right). \quad (\text{S9})$$

Provided that the ground state of \hat{H} is nondegenerate, take the limit $T \rightarrow \infty$, and then terms on the right hand side (RHS) vanish except for ΔE , viz.,

$$\lim_{T \rightarrow \infty} \frac{i}{T - i\eta} \ln \langle \hat{U}(\frac{T - i\eta}{2}, -\frac{T - i\eta}{2}) \rangle_0 = \Delta E \quad (\text{S10})$$

Taking the limit $\lim_{\eta \rightarrow 0^+}$, we reach an expression for the perturbative correction to the ground state energy

$$\Delta E = \lim_{\eta \rightarrow 0^+} \lim_{T \rightarrow \infty} \frac{i}{T - i\eta} \ln \langle \hat{U}(\frac{T - i\eta}{2}, -\frac{T - i\eta}{2}) \rangle_0 = \lim_{T \rightarrow \infty} \frac{i}{T} \ln \langle \hat{U}(\frac{T}{2}, -\frac{T}{2}) \rangle_0, \quad (\text{S11})$$

where in the second equality, we omitted η for simplicity. In the following derivations, we will always implicitly assume that T is on the contour, and the limit $\eta \rightarrow 0^+$ will be taken in the final expression.

Interpreting $\langle \hat{U}(\frac{T}{2}, -\frac{T}{2}) \rangle_0$ as the moment generating function for the moments μ_n in Eq. (5), then $\ln \langle \hat{U}(\frac{T}{2}, -\frac{T}{2}) \rangle_0 = \sum_{n=1} \frac{\lambda^n}{n!} \kappa_n$ is the corresponding cumulant generating function for the cumulants κ_n . This allows to identify the n -th order energy correction ΔE_n from Eq. (4) simply as

$$\Delta E_n = \lim_{T \rightarrow \infty} \frac{i}{T n!} \kappa_n, \quad n \geq 1. \quad (\text{S12})$$

The connection of the energy correction to cumulant reveals the size-extensivity[68] of ΔE_n , and can be viewed a generalization of the linked cluster theorem in standard MBPT[50, 69].

B. Proof of the MR-RPA correlation energy - Eq. (9)

In the n -th order energy correction (7), we consider the two-body perturbation defined in Eq. (3),

$$\langle \mathcal{T}[\hat{V}_I(t_1)\hat{V}_I(t_2) \cdots \hat{V}_I(t_n)] \rangle_0 = \frac{1}{2^n} \prod_{i=1}^n v_{p_{2i-1}r_{2i-1}, p_{2i}r_{2i}} \langle \mathcal{T}[\prod_{i=1}^n \hat{p}_{2i-1}^\dagger(t_i)\hat{r}_{2i-1}(t_i)\hat{p}_{2i}^\dagger(t_i)\hat{r}_{2i}(t_i)] \rangle_0, \quad (\text{S13})$$

where $\hat{p}^\dagger(t) = e^{i\hat{H}_0 t} \hat{p}^\dagger e^{-i\hat{H}_0 t}$ and the Einstein summation convention has been implied for repeated orbital indices. The expectation value of the product of creation/annihilation operators on the RHS of Eq. (S13) can be expanded using the cumulant expansion of time-ordered Green's function[5, 49], which will generate many different contraction patterns. Here, we focus on a specific kind of contraction patterns, which can be viewed as a generalization of the ring diagrams (see Fig. 1(b)). In such ring diagrams, the two interaction vertices are connected either by two Green function lines as in conventional SR-RPA,

$$\langle \mathcal{T}[\hat{p}_i^\dagger(t_i)\hat{r}_j(t_j)] \rangle_0 \langle \mathcal{T}[\hat{r}_i(t_i)\hat{p}_j^\dagger(t_j)] \rangle_0 = - \langle \mathcal{T}[\hat{r}_j(t_j)\hat{p}_i^\dagger(t_i)] \rangle_0 \langle \mathcal{T}[\hat{r}_i(t_i)\hat{p}_j^\dagger(t_j)] \rangle_0 = G_{r_j p_i}^0(t_j, t_i) G_{r_i p_j}^0(t_i, t_j), \quad (\text{S14})$$

or by a two-body connected Green's function

$$\langle \mathcal{T}[\hat{p}_i^\dagger(t_i^+)\hat{r}_i(t_i)\hat{p}_j^\dagger(t_j^+)\hat{r}_j(t_j)] \rangle_{0,c} = \langle \mathcal{T}[\hat{r}_i(t_i)\hat{r}_j(t_j)\hat{p}_j^\dagger(t_j^+)\hat{p}_i^\dagger(t_i^+)] \rangle_{0,c} \equiv -G_{r_i r_j, p_i p_j}^{0,c}(t_i, t_j, t_i^+, t_j^+). \quad (\text{S15})$$

The sum of these two contributions gives

$$\begin{aligned}
& G_{r_j p_i}^0(t_j, t_i) G_{r_i p_j}^0(t_i, t_j) - G_{r_i r_j, p_i p_j}^{0,c}(t_i, t_j, t_i^+, t_j^+) \\
&= G_{r_j p_i}^0(t_j, t_i) G_{r_i p_j}^0(t_i, t_j) - \left[G_{r_i r_j, p_i p_j}^0(t_i, t_j, t_i^+, t_j^+) - G_{r_i p_i}^0(t_i, t_i^+) G_{r_j p_j}^0(t_j, t_j^+) + G_{r_i p_j}^0(t_i, t_j) G_{r_j p_i}^0(t_j, t_i) \right] \\
&= -G_{r_i r_j, p_i p_j}^0(t_i, t_j, t_i^+, t_j^+) + G_{r_i p_i}^0(t_i, t_i^+) G_{r_j p_j}^0(t_j, t_j^+) \\
&= \langle \mathcal{T} [\hat{p}_i^\dagger(t_i^+) \hat{r}_i(t_i) \hat{p}_j^\dagger(t_j^+) \hat{r}_j(t_j)] \rangle_0 - \langle \hat{p}_i^\dagger \hat{r}_i \rangle_0 \langle \hat{p}_j^\dagger \hat{r}_j \rangle_0 \\
&= \langle \mathcal{T} \left[\left(\hat{p}_i^\dagger(t_i^+) \hat{r}_i(t_i) - \langle \hat{p}_i^\dagger \hat{r}_i \rangle_0 \right) \left(\hat{p}_j^\dagger(t_j^+) \hat{r}_j(t_j) - \langle \hat{p}_j^\dagger \hat{r}_j \rangle_0 \right) \right] \rangle_0 \equiv L_{p_i r_i, p_j r_j}^0(t_i, t_j). \tag{S16}
\end{aligned}$$

Then, the n -th order energy defined by generalized ring diagrams in Fig. 1(b) can be expressed as

$$\begin{aligned}
\Delta E_n^{\text{ring}} &= \lim_{T \rightarrow \infty} \frac{i}{T} \frac{(-i)^n}{2n} \int_{-\frac{T}{2}}^{\frac{T}{2}} dt_1 \int_{-\frac{T}{2}}^{\frac{T}{2}} dt_2 \cdots \int_{-\frac{T}{2}}^{\frac{T}{2}} dt_n v_{p_1 r_1, p_2 r_2} L_{p_2 r_2, p_3 r_3}^0(t_1, t_2) \\
&\quad v_{p_3 r_3, p_4 r_4} L_{p_4 r_4, p_5 r_5}^0(t_2, t_3) \cdots v_{p_{2n-1} r_{2n-1}, p_{2n} r_{2n}} L_{p_{2n} r_{2n}, p_1 r_1}^0(t_n, t_1), \tag{S17}
\end{aligned}$$

where the factor $\frac{1}{2n}$ originates from the symmetry factor of diagrams. Now using $\Pi_{p_i r_i, p_j r_j}^0(t_1, t_2) = -i L_{p_i r_i, p_j r_j}^0(t_1, t_2)$ (8), the above expression can be written as

$$\Delta E_n^{\text{ring}} = \lim_{T \rightarrow \infty} \frac{i}{T} \frac{1}{2n} \int_{-\frac{T}{2}}^{\frac{T}{2}} dt_1 \int_{-\frac{T}{2}}^{\frac{T}{2}} dt_2 \cdots \int_{-\frac{T}{2}}^{\frac{T}{2}} dt_n \text{tr}[\mathbf{v} \mathbf{\Pi}^0(t_1, t_2) \mathbf{v} \mathbf{\Pi}^0(t_2, t_3) \cdots \mathbf{v} \mathbf{\Pi}^0(t_n, t_1)]. \tag{S18}$$

Using the Fourier transform to the frequency domain (see p150 of Ref. [5]) leads to a compact expression

$$\Delta E_n^{\text{ring}} = \frac{i}{2n} \int_{-\infty}^{+\infty} \frac{d\omega}{2\pi} \text{tr}([\mathbf{v} \mathbf{\Pi}^0(\omega)]^n), \tag{S19}$$

with $\mathbf{\Pi}(\omega)$ given by

$$\Pi_{p_i r_i, p_j r_j}^0(\omega) = (-i) \int_{-\infty}^{+\infty} d\tilde{t} e^{i\omega \tilde{t}} L_{p_i r_i, p_j r_j}^0(t, 0) \quad [t = (1 - i\eta)\tilde{t}] \tag{S20}$$

$$= (-i) \int_{-\infty}^{+\infty} d\tilde{t} e^{i\omega \tilde{t}} \left[\langle \mathcal{T} [\hat{p}_i^\dagger(t^+) \hat{r}_i(t) \hat{p}_j^\dagger \hat{r}_j] \rangle_0 - \langle \hat{p}_i^\dagger \hat{r}_i \rangle_0 \langle \hat{p}_j^\dagger \hat{r}_j \rangle_0 \right] \tag{S21}$$

$$\begin{aligned}
&= (-i) \int_{-\infty}^{+\infty} d\tilde{t} e^{i\omega \tilde{t}} \left[\theta(\tilde{t}) \langle \hat{p}_i^\dagger \hat{r}_i e^{-i(\hat{H}_0 - E_0^{(0)})\tilde{t}} \hat{p}_j^\dagger \hat{r}_j \rangle_0 \right. \\
&\quad \left. + \theta(-\tilde{t}) \langle \hat{p}_j^\dagger \hat{r}_j e^{i(\hat{H}_0 - E_0^{(0)})\tilde{t}} \hat{p}_i^\dagger \hat{r}_i \rangle_0 - \langle \hat{p}_i^\dagger \hat{r}_i \rangle_0 \langle \hat{p}_j^\dagger \hat{r}_j \rangle_0 \right] \tag{S22}
\end{aligned}$$

$$\begin{aligned}
&= (-i) \left[\sum_{N>0} \int_0^{+\infty} d\tilde{t} e^{i(\omega - \omega_N(1-i\eta))\tilde{t}} \langle 0 | \hat{p}_i^\dagger \hat{r}_i | N \rangle \langle N | \hat{p}_j^\dagger \hat{r}_j | 0 \rangle \right. \\
&\quad \left. + \sum_{N>0} \int_{-\infty}^0 d\tilde{t} e^{i(\omega + \omega_N(1-i\eta))\tilde{t}} \langle 0 | \hat{p}_j^\dagger \hat{r}_j | N \rangle \langle N | \hat{p}_i^\dagger \hat{r}_i | 0 \rangle \right] \tag{S23}
\end{aligned}$$

$$= \sum_{N>0} \frac{\langle 0 | \hat{p}_i^\dagger \hat{r}_i | N \rangle \langle N | \hat{p}_j^\dagger \hat{r}_j | 0 \rangle}{\omega - \omega_N + i\eta} - \sum_{N>0} \frac{\langle 0 | \hat{p}_j^\dagger \hat{r}_j | N \rangle \langle N | \hat{p}_i^\dagger \hat{r}_i | 0 \rangle}{\omega + \omega_N - i\eta}, \tag{S24}$$

where $|0\rangle$ and $|N\rangle$ are shorthand notations for $|\Phi_0\rangle$ and $|\Phi_N\rangle$, respectively, and $\omega_N = E_N^{(0)} - E_0^{(0)}$.

Using the special contour shown in Fig. S1 and the property that the integrand decays as $1/\omega^n$ ($n \geq 2$) in Eq. (S19), we can change the integration over real frequency to imaginary frequency

$$\Delta E_n^{\text{ring}} = -\frac{1}{2n} \frac{1}{2\pi} \int_{-\infty}^{+\infty} d\omega \text{tr}([\mathbf{v} \mathbf{\Pi}^0(i\omega)]^n), \tag{S25}$$

which is more amenable for numerical evaluations using quadrature. Finally, the MR-RPA correlation energy (9) can be obtained as

$$\Delta E^{\text{RPA}} = \sum_{n \geq 2} \Delta E_n^{\text{ring}} = \sum_{n \geq 2} -\frac{1}{2n} \int_{-\infty}^{+\infty} \frac{d\omega}{2\pi} \text{tr}([\mathbf{v} \mathbf{\Pi}^0(i\omega)]^n) = \int_{-\infty}^{+\infty} \frac{d\omega}{2\pi} \frac{1}{2} \text{tr} [\ln[\mathbf{I} - \mathbf{v} \mathbf{\Pi}^0(i\omega)] + \mathbf{v} \mathbf{\Pi}^0(i\omega)]. \tag{S26}$$

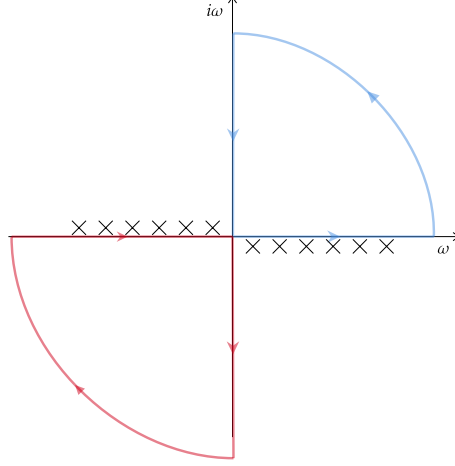


FIG. S1. Contour used to change the integration over real frequency to imaginary frequency. The crosses represent the poles of $\Pi^0_{p_i r_i, p_j q_j}(\omega)$.

C. Proof of the plasmon formula - Eq. (12)

Substituting $\frac{1}{n}$ with the identity $\frac{1}{n} = \int_0^1 d\lambda \lambda^{n-1}$ in Eq. (S26), we obtain

$$\begin{aligned} \Delta E^{\text{RPA}} &= -\frac{1}{2} \sum_{n \geq 2} \int_0^1 d\lambda \int_{-\infty}^{+\infty} \frac{d\omega}{2\pi} \lambda^{n-1} \text{tr}([\mathbf{v}\mathbf{\Pi}^0(i\omega)]^n) \\ &= -\frac{1}{2} \int_0^1 d\lambda \int_{-\infty}^{+\infty} \frac{d\omega}{2\pi} \text{tr}(\mathbf{v}[\mathbf{\Pi}^\lambda(i\omega) - \mathbf{\Pi}^0(i\omega)]), \end{aligned} \quad (\text{S27})$$

with $\mathbf{\Pi}^\lambda(z)$ given in Eq. (10). Now we show that Eq. (S27) can be transformed into the plasmon formula as in SR-RPA[14]. To this end, the key observation is that Eq. (S24) can be written as a product of two vectors and a diagonal matrix, viz.,

$$\mathbf{\Pi}^0_{pr,qs}(z) = (\langle 0|\hat{p}^\dagger \hat{r}|M\rangle \quad \langle M|\hat{p}^\dagger \hat{r}|0\rangle) \begin{pmatrix} (z - \omega_N)^{-1} \delta_{MN} & 0 \\ 0 & -(z + \omega_N)^{-1} \delta_{MN} \end{pmatrix} \begin{pmatrix} \langle N|\hat{q}^\dagger \hat{s}|0\rangle \\ \langle 0|\hat{q}^\dagger \hat{s}|N\rangle \end{pmatrix}, \quad (\text{S28})$$

where the Einstein summation convention has been implied for repeated indices $M, N > 0$. Then, we can introduce two auxiliary matrices $\mathbf{D}^0(z)$ and \mathbf{V} defined by

$$\mathbf{D}^0(z) = -[\mathbf{\Delta} - z\mathbf{S}]^{-1}, \quad \mathbf{\Delta} = \begin{pmatrix} \omega & \mathbf{0} \\ \mathbf{0} & \omega \end{pmatrix}, \quad \mathbf{S} = \begin{pmatrix} \mathbf{I} & \mathbf{0} \\ \mathbf{0} & -\mathbf{I} \end{pmatrix}, \quad (\text{S29})$$

and

$$\mathbf{V} = \begin{pmatrix} \mathbf{V}^{11} & \mathbf{V}^{12} \\ \mathbf{V}^{21} & \mathbf{V}^{22} \end{pmatrix} = \begin{pmatrix} \mathbf{V}^{11} & \mathbf{V}^{12} \\ \mathbf{V}^{12*} & \mathbf{V}^{11*} \end{pmatrix}, \quad (\text{S30})$$

$$V_{NM}^{11} = \langle N|\hat{p}^\dagger \hat{r}|0\rangle v_{pr,qs} \langle 0|\hat{q}^\dagger \hat{s}|M\rangle, \quad (\text{S31})$$

$$V_{NM}^{12} = \langle N|\hat{p}^\dagger \hat{r}|0\rangle v_{pr,qs} \langle M|\hat{q}^\dagger \hat{s}|0\rangle, \quad (\text{S32})$$

$$V_{NM}^{21} = \langle 0|\hat{p}^\dagger \hat{r}|N\rangle v_{pr,qs} \langle 0|\hat{q}^\dagger \hat{s}|M\rangle, \quad (\text{S33})$$

$$V_{NM}^{22} = \langle 0|\hat{p}^\dagger \hat{r}|N\rangle v_{pr,qs} \langle M|\hat{q}^\dagger \hat{s}|0\rangle, \quad (\text{S34})$$

such that

$$\text{tr}([\mathbf{v}\mathbf{\Pi}^0(z)]^n) = \text{tr}([\mathbf{V}\mathbf{D}^0(z)]^n), \quad (\text{S35})$$

which allows us to rewrite Eq. (S27) as

$$\Delta E^{\text{RPA}} = -\frac{1}{2} \int_0^1 d\lambda \int_{-\infty}^{\infty} \frac{d\omega}{2\pi} \text{tr}(\mathbf{v}[\mathbf{\Pi}^\lambda(i\omega) - \mathbf{\Pi}^0(i\omega)]) = -\frac{1}{2} \int_0^1 d\lambda \int_{-\infty}^{\infty} \frac{d\omega}{2\pi} \text{tr}(\mathbf{V}[\mathbf{D}^\lambda(i\omega) - \mathbf{D}^0(i\omega)]), \quad (\text{S36})$$

with

$$\mathbf{D}^\lambda(z) = \mathbf{D}^0(z) + \lambda \mathbf{D}^0(z) \mathbf{V} \mathbf{D}^\lambda(z), \quad (\text{S37})$$

analogous to Eq. (10) for $\mathbf{\Pi}^\lambda(z)$. Unlike $\mathbf{\Pi}^0(z)$, $\mathbf{D}^0(z)$ is a diagonal matrix similar to the SR-RPA case. Thus, we can follow the derivation of the plasmon formula in SR-RPA[14] using $\mathbf{D}^0(z)$ and \mathbf{V} .

To integrate over λ and ω in Eq. (S36) analytically, it is crucial to find the spectral representation of $\mathbf{D}^\lambda(z)$. We first rewrite $\mathbf{D}^\lambda(z)$ as

$$\mathbf{D}^\lambda(z) = ([\mathbf{D}^0(z)]^{-1} - \lambda \mathbf{V})^{-1} = -(\mathbf{\Delta} + \lambda \mathbf{V} - z \mathbf{S})^{-1} \equiv -(\mathbf{E}^\lambda - z \mathbf{S})^{-1} \quad (\text{S38})$$

where

$$\mathbf{E}^\lambda \equiv \mathbf{\Delta} + \lambda \mathbf{V} = \begin{pmatrix} \omega + \lambda \mathbf{V}_{11} & \lambda \mathbf{V}_{12} \\ \lambda \mathbf{V}_{12}^* & \omega + \lambda \mathbf{V}_{11}^* \end{pmatrix} \equiv \begin{pmatrix} \mathbf{A}^\lambda & \mathbf{B}^\lambda \\ \mathbf{B}^{\lambda*} & \mathbf{A}^{\lambda*} \end{pmatrix}. \quad (\text{S39})$$

Then, we can solve the eigenvalue problem

$$\mathbf{E}^\lambda \mathbf{u}^\lambda = z \mathbf{S} \mathbf{u}^\lambda. \quad (\text{S40})$$

The structure of \mathbf{E}^λ implies that its eigensystem has a paired structure as in SR-RPA, viz., the eigenvalues $\pm \Omega_I^\lambda$ appear in pairs with the corresponding eigenvectors given by

$$\mathbf{u}_I^\lambda = \begin{pmatrix} \mathbf{x}_I \\ \mathbf{y}_I \end{pmatrix}, \quad \mathbf{u}_{-I}^\lambda = \begin{pmatrix} \mathbf{y}_I^* \\ \mathbf{x}_I^* \end{pmatrix}. \quad (\text{S41})$$

Collecting all the eigenvectors into a matrix $\mathbf{U}^\lambda = [\cdots \mathbf{u}_I^\lambda \cdots, \cdots \mathbf{u}_{-I}^\lambda \cdots]$, we have

$$(\mathbf{U}^\lambda)^\dagger \mathbf{E}^\lambda \mathbf{U}^\lambda = \begin{pmatrix} \Omega_I^\lambda \delta_{IJ} & 0 \\ 0 & \Omega_I^\lambda \delta_{IJ} \end{pmatrix} \equiv \mathbf{\Omega}^\lambda, \quad (\mathbf{U}^\lambda)^\dagger \mathbf{S} \mathbf{U}^\lambda = \begin{pmatrix} \delta_{IJ} & 0 \\ 0 & -\delta_{IJ} \end{pmatrix} = \mathbf{S}. \quad (\text{S42})$$

The latter is the normalization condition[25]. Then, the spectral representation of $\mathbf{D}^\lambda(z)$ can be expressed as

$$\begin{aligned} \mathbf{D}^\lambda(z) &= -(\mathbf{E}^\lambda - z \mathbf{S})^{-1} = -\mathbf{U}^\lambda (\mathbf{\Omega}^\lambda - z \mathbf{S})^{-1} (\mathbf{U}^\lambda)^\dagger \\ &= - \left[\sum_{I>0} \frac{\mathbf{u}_I^\lambda \mathbf{u}_I^{\lambda\dagger}}{\Omega_I^\lambda - z} + \sum_{I>0} \frac{\mathbf{u}_{-I}^\lambda \mathbf{u}_{-I}^{\lambda\dagger}}{\Omega_I^\lambda + z} \right]. \end{aligned} \quad (\text{S43})$$

Now we can integrate out both λ and ω in Eq. (S36) analytically. Specifically, the first term becomes

$$\begin{aligned} & -\frac{1}{2} \int_0^1 d\lambda \int_{-\infty}^{\infty} \frac{d\omega}{2\pi} \text{tr}(\mathbf{v} \mathbf{\Pi}^\lambda(i\omega)) = -\frac{1}{2} \int_0^1 d\lambda \int_{-\infty}^{\infty} \frac{d\omega}{2\pi} \text{tr}(\mathbf{V} \mathbf{D}^\lambda(i\omega)) \\ &= \frac{1}{2} \int_0^1 d\lambda \int_{-\infty}^{\infty} \frac{d\omega}{2\pi} \left[\sum_{I>0} \frac{\mathbf{u}_I^{\lambda\dagger} \mathbf{V} \mathbf{u}_I^\lambda}{\Omega_I - i\omega} + \sum_{I>0} \frac{\mathbf{u}_{-I}^{\lambda\dagger} \mathbf{V} \mathbf{u}_{-I}^\lambda}{\Omega_I + i\omega} \right] \\ &= \frac{1}{2} \int_0^1 d\lambda \int_{-\infty}^{\infty} \frac{d\omega}{2\pi} \sum_{I>0} \mathbf{u}_I^{\lambda\dagger} \mathbf{V} \mathbf{u}_I^\lambda \frac{2\Omega_I}{\Omega_I^2 + \omega^2} \\ &= \frac{1}{2} \int_0^1 d\lambda \sum_{I>0} \mathbf{u}_I^{\lambda\dagger} \mathbf{V} \mathbf{u}_I^\lambda = \frac{1}{2} \int_0^1 d\lambda \sum_{I>0} \frac{d\Omega_I^\lambda}{d\lambda} \\ &= \frac{1}{2} \sum_{I>0} (\Omega_I^{\lambda=1} - \Omega_I^{\lambda=0}), \end{aligned} \quad (\text{S44})$$

where the third equality follows from $\mathbf{u}_I^{\lambda\dagger} \mathbf{V} \mathbf{u}_I^\lambda = \mathbf{u}_I^{\lambda T} \mathbf{V}^* \mathbf{u}_I^{\lambda*} = \mathbf{u}_{-I}^{\lambda\dagger} \mathbf{V} \mathbf{u}_{-I}^\lambda$, in which the paired structure (S41) is employed, and the second last equality follows from the Hellman-Feynman theorem. Likewise, the second term in Eq. (S36) can be rewritten as

$$\begin{aligned} & \frac{1}{2} \int_0^1 d\lambda \int_{-\infty}^{\infty} \frac{d\omega}{2\pi} \text{tr}(\mathbf{v} \mathbf{\Pi}^0(i\omega)) = \frac{1}{2} \int_{-\infty}^{\infty} \frac{d\omega}{2\pi} \text{tr}(\mathbf{V} \mathbf{D}^0(i\omega)) \\ & = -\frac{1}{2} \int_{-\infty}^{\infty} \frac{d\omega}{2\pi} \sum_{N>0} V_{NN}^{11} \left[\frac{1}{\omega_{N0} - i\omega} + \frac{1}{\omega_{N0} + i\omega} \right] \\ & = -\frac{1}{2} \sum_{N>0} V_{NN}^{11} = -\frac{1}{2} \text{tr}(\mathbf{V}^{11}). \end{aligned} \quad (\text{S45})$$

Finally, Eq. (S27) becomes

$$\begin{aligned} \Delta E^{\text{RPA}} &= -\frac{1}{2} \int_0^1 d\lambda \int_{-\infty}^{\infty} \frac{d\omega}{2\pi} \text{tr}(\mathbf{v} [\mathbf{\Pi}^\lambda(i\omega) - \mathbf{\Pi}^0(i\omega)]) \\ &= \frac{1}{2} \sum_{I>0} (\Omega_I^{\lambda=1} - \Omega_I^{\lambda=0}) - \frac{1}{2} \text{tr}(\mathbf{V}_{11}) \\ &= \frac{1}{2} \left(\sum_{I>0} \Omega_I^{\lambda=1} - \text{tr}(\mathbf{A}) \right) \\ &= \frac{1}{2} \sum_{I>0} (\Omega_I^{\text{RPA}} - \Omega_I^{\text{TDA}}), \end{aligned} \quad (\text{S46})$$

where we have used the invariance of the trace $\sum_{I>0} \Omega_I^{\text{TDA}} = \text{tr}(\mathbf{A})$. This completes the proof of Eq. (12).

D. Connection to coupled-cluster theory

To obtain MR-SOSEX in the main text, we follow the connection of the RPA eigenvalue problem with the coupled-cluster equation developed for SR-RPA[23]. In this subsection, we further elaborate this connection in details.

Starting from Eq. (13), we collect all the eigenvectors with positive eigenvalues into square matrices \mathbf{X} and \mathbf{Y} , such that

$$\begin{pmatrix} \mathbf{A} & \mathbf{B} \\ \mathbf{B}^* & \mathbf{A}^* \end{pmatrix} \begin{pmatrix} \mathbf{X} \\ \mathbf{Y} \end{pmatrix} = \begin{pmatrix} \mathbf{I} & \mathbf{0} \\ \mathbf{0} & -\mathbf{I} \end{pmatrix} \begin{pmatrix} \mathbf{X} \\ \mathbf{Y} \end{pmatrix} \mathbf{\Omega}, \quad (\text{S47})$$

where $\mathbf{\Omega}$ is a diagonal matrix containing all the corresponding positive eigenvalues. Following Ref. [23], we can define

$$\mathbf{T} \equiv \mathbf{Y} \mathbf{X}^{-1}, \quad \mathbf{R} \equiv \mathbf{X} \mathbf{\Omega} \mathbf{X}^{-1}. \quad (\text{S48})$$

Right multiplying Eq. (S47) by \mathbf{X}^{-1} leads to

$$\begin{pmatrix} \mathbf{A} & \mathbf{B} \\ \mathbf{B}^* & \mathbf{A}^* \end{pmatrix} \begin{pmatrix} \mathbf{I} \\ \mathbf{T} \end{pmatrix} = \begin{pmatrix} \mathbf{I} & \mathbf{0} \\ \mathbf{0} & -\mathbf{I} \end{pmatrix} \begin{pmatrix} \mathbf{I} \\ \mathbf{T} \end{pmatrix} \mathbf{R}, \quad (\text{S49})$$

or equivalently

$$\mathbf{A} + \mathbf{B} \mathbf{T} = \mathbf{R}, \quad (\text{S50})$$

$$\mathbf{B}^* + \mathbf{A}^* \mathbf{T} = -\mathbf{T} \mathbf{R}. \quad (\text{S51})$$

Eq. (S50) allows us to rewrite the RPA correlation energy as

$$\Delta E = \frac{1}{2} \sum_{I>0} (\Omega_I^{\text{RPA}} - \Omega_I^{\text{TDA}}) = \frac{1}{2} \text{tr}(\mathbf{R} - \mathbf{A}) = \frac{1}{2} \text{tr}(\mathbf{B} \mathbf{T}). \quad (\text{S52})$$

Eliminating \mathbf{R} from Eq. (S51) using Eq. (S50) leads to a quadratic equation for \mathbf{T} ,

$$\mathbf{B}^* + \mathbf{A}^* \mathbf{T} + \mathbf{T} \mathbf{A} + \mathbf{T} \mathbf{B} \mathbf{T} = \mathbf{0}. \quad (\text{S53})$$

In the single-reference case, this equation is identical to the drCCD equation for the double excitation amplitude $t_{ai,bj}$. In the multi-reference case, the situation is more complicated. To the best of our knowledge, the corresponding equation (S53) for MR-RPA does not correspond to any existing multi-reference coupled-cluster theory. Whether Eq. (S53) can be derived from a novel multi-reference coupled-cluster theory is an intriguing question, and is currently being explored.

S2. MATRIX ELEMENTS OF MR-RPA WITH A CASSCF REFERENCE

The molecular spin-orbitals for a CASSCF reference are partitioned into three parts: core (viz. closed shell) $\{i, j, \dots\}$, virtual $\{a, b, \dots\}$ and active $\{x, y, \dots\}$ orbitals, see Fig. S2. After CASSCF calculations, the core and virtual orbitals are canonicalized by diagonalizing the following Fock matrices

$$F_{ij} = h_{ij} + \langle ik || jk \rangle + \langle ix || jy \rangle \gamma_{xy} = \epsilon_i \delta_{ij}, \quad (\text{S54})$$

$$F_{ab} = h_{ab} + \langle ak || bk \rangle + \langle ax || by \rangle \gamma_{xy} = \epsilon_a \delta_{ab}, \quad (\text{S55})$$

which define ϵ_i and ϵ_a in the Dyall Hamiltonian (19). Here, $\langle pq || rs \rangle = \langle pq | rs \rangle - \langle pq | sr \rangle = (pr | qs) - (ps | qr)$ is the antisymmetrized two-electron integral, $(pr | qs)$ is the two-electron integral $\langle pq | rs \rangle$ in the so-called chemists' notation[3], and $\gamma_{xy} = \langle \Phi_0^{NA} | \hat{x}^\dagger \hat{y} | \Phi_0^{NA} \rangle$ is the one-particle density matrix of the CASSCF active space wavefunction. Different from F_{ij} and F_{ab} , f_{xy} in Eq. (20) is defined as a mean-field only generated by the core electrons

$$f_{xy} = h_{xy} + \langle xk || yk \rangle, \quad (\text{S56})$$

which avoids the double counting of electron-electron interactions among the active orbitals, since they have been explicitly taken into account in the second term of Eq. (20). As a result, the two-electron perturbation $v_{pr,qs}$ defined in Eq. (3) for \hat{H}_D has a simple block structure, namely, the block involving four active indices vanishes ($v_{xz,yw} = 0$), while all other blocks retain the original Coulomb interaction, e.g., $v_{xi,ay} = (xi | ay)$.

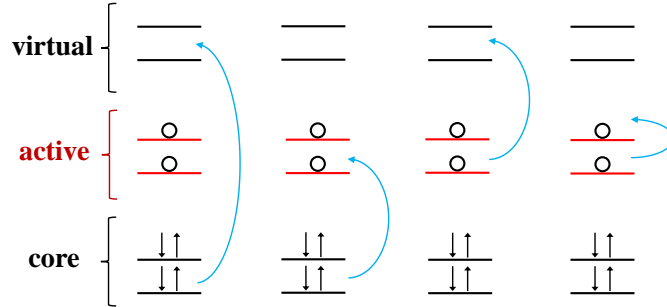


FIG. S2. Schematic representation of the four classes of zeroth-order excited states that contribute in the MR-RPA theory with a CASSCF reference and the Dyall Hamiltonian, see Eq. (21). The circles on active orbitals mean that the occupation number is between $[0, 2]$.

As shown in Eq. (21) and illustrated in Fig. S2, there are four classes of zeroth-order excited states $|N\rangle$, which can make $\langle N | \hat{p}^\dagger \hat{r} | 0 \rangle$ nonzero, and hence contribute to the MR-RPA theory with a CASSCF reference and the Dyall Hamiltonian[56]. As a result, \mathbf{A} (14) and \mathbf{B} (15) have the following block structure:

$$\mathbf{A} = \begin{pmatrix} [A_{ai,bj}] & [A_{ai,\nu j}] & [A_{ai,b\nu}] & [A_{ai,\nu}] \\ [A_{\mu i,bj}] & [A_{\mu i,\nu j}] & [A_{\mu i,b\nu}] & [A_{\mu i,\nu}] \\ [A_{a\mu,bj}] & [A_{a\mu,\nu j}] & [A_{a\mu,b\nu}] & [A_{a\mu,\nu}] \\ [A_{\mu,bj}] & [A_{\mu,\nu j}] & [A_{\mu,b\nu}] & [A_{\mu,\nu}] \end{pmatrix}, \quad \mathbf{B} = \begin{pmatrix} [B_{ai,bj}] & [B_{ai,\nu j}] & [B_{ai,b\nu}] & [B_{ai,\nu}] \\ [B_{\mu i,bj}] & [B_{\mu i,\nu j}] & [B_{\mu i,b\nu}] & [B_{\mu i,\nu}] \\ [B_{a\mu,bj}] & [B_{a\mu,\nu j}] & [B_{a\mu,b\nu}] & [B_{a\mu,\nu}] \\ [B_{\mu,bj}] & [B_{\mu,\nu j}] & [B_{\mu,b\nu}] & [B_{\mu,\nu}] \end{pmatrix}. \quad (\text{S57})$$

It is easy to show that \mathbf{A} is Hermitian and \mathbf{B} is symmetric. Thus, only 10 of 16 blocks in \mathbf{A} and \mathbf{B} are independent. Calculation of the first term in Eq. (14) for \mathbf{A} can be simplified by noting the additively separable structure of \hat{H}_D , such that the active space Hamiltonian \hat{H}_A can be diagonalized in a subspace with a given number of electrons:

$$\hat{H}_A |\Phi_\mu^N\rangle = E_\mu^N |\Phi_\mu^N\rangle, \quad (\text{S58})$$

where E_μ^N and $|\Phi_\mu^N\rangle$ are the μ -th eigenvalue and wavefunction of \hat{H}_A with N electrons in the active space $\text{CAS}(N, M_A)$, respectively. The zeroth-order excitation energies in Eq. (14) are

$$\omega_\mu^N = E_\mu^N - E_0^{N_A}, \quad (\text{S59})$$

where $E_0^{N_A}$ is the energy of the ground state $|\Phi_0^{N_A}\rangle$ of \hat{H}_A with N_A electrons. The lower triangular blocks of A_{NM} and B_{NM} in Eq. (S57) are given as follows:

$$1. |N\rangle = |\Theta_i^a\rangle|\Phi_0^{N_A}\rangle, |M\rangle = |\Theta_j^b\rangle|\Phi_0^{N_A}\rangle$$

$$A_{ai,bj} = (\epsilon_a - \epsilon_i)\delta_{ij}\delta_{ab} + (ai|jb), \quad (\text{S60})$$

$$B_{ai,bj} = (ai|bj), \quad (\text{S61})$$

$$2. |N\rangle = |\Theta_i\rangle|\Phi_\mu^{N_A+1}\rangle, |M\rangle = |\Theta_j^b\rangle|\Phi_0^{N_A}\rangle$$

$$A_{\mu i,bj} = (-1)\langle\Phi_\mu^{N_A+1}|\hat{x}^\dagger|\Phi_0^{N_A}\rangle(xi|jb), \quad (\text{S62})$$

$$B_{\mu i,bj} = (-1)\langle\Phi_\mu^{N_A+1}|\hat{x}^\dagger|\Phi_0^{N_A}\rangle(xi|bj), \quad (\text{S63})$$

$$3. |N\rangle = |\Theta_i\rangle|\Phi_\mu^{N_A+1}\rangle, |M\rangle = |\Theta_j\rangle|\Phi_\nu^{N_A+1}\rangle$$

$$A_{\mu i,\nu j} = (\omega_\mu^{N_A+1} - \epsilon_i)\delta_{ij}\delta_{\mu\nu} + \langle\Phi_\mu^{N_A+1}|\hat{x}^\dagger|\Phi_0^{N_A}\rangle(xi|jy)\langle\Phi_0^{N_A}|\hat{y}|\Phi_\nu^{N_A+1}\rangle, \quad (\text{S64})$$

$$B_{\mu i,\nu j} = \langle\Phi_\mu^{N_A+1}|\hat{x}^\dagger|\Phi_0^{N_A}\rangle(xi|yj)\langle\Phi_\nu^{N_A+1}|\hat{y}^\dagger|\Phi_0^{N_A}\rangle, \quad (\text{S65})$$

$$4. |N\rangle = |\Theta^a\rangle|\Phi_\mu^{N_A-1}\rangle, |M\rangle = |\Theta_j^b\rangle|\Phi_0^{N_A}\rangle$$

$$A_{a\mu,bj} = \langle\Phi_\mu^{N_A-1}|\hat{x}|\Phi_0^{N_A}\rangle(ax|jb), \quad (\text{S66})$$

$$B_{a\mu,bj} = \langle\Phi_\mu^{N_A-1}|\hat{x}|\Phi_0^{N_A}\rangle(ax|bj), \quad (\text{S67})$$

$$5. |N\rangle = |\Theta^a\rangle|\Phi_\mu^{N_A-1}\rangle, |M\rangle = |\Theta_j\rangle|\Phi_\nu^{N_A+1}\rangle$$

$$A_{a\mu,\nu j} = (-1)\langle\Phi_\mu^{N_A-1}|\hat{x}|\Phi_0^{N_A}\rangle(ax|jy)\langle\Phi_0^{N_A}|\hat{y}|\Phi_\nu^{N_A+1}\rangle, \quad (\text{S68})$$

$$B_{a\mu,\nu j} = (-1)\langle\Phi_\mu^{N_A-1}|\hat{x}|\Phi_0^{N_A}\rangle(ax|yj)\langle\Phi_\nu^{N_A+1}|\hat{y}^\dagger|\Phi_0^{N_A}\rangle, \quad (\text{S69})$$

$$6. |N\rangle = |\Theta^a\rangle|\Phi_\mu^{N_A-1}\rangle, |M\rangle = |\Theta^b\rangle|\Phi_\nu^{N_A-1}\rangle$$

$$A_{a\mu,b\nu} = (\omega_\mu^{N_A-1} + \epsilon_a)\delta_{ab}\delta_{\mu\nu} + \langle\Phi_\mu^{N_A-1}|\hat{x}|\Phi_0^{N_A}\rangle(ax|yb)\langle\Phi_0^{N_A}|\hat{y}^\dagger|\Phi_\nu^{N_A-1}\rangle, \quad (\text{S70})$$

$$B_{a\mu,b\nu} = \langle\Phi_\mu^{N_A-1}|\hat{x}|\Phi_0^{N_A}\rangle(ax|by)\langle\Phi_\nu^{N_A-1}|\hat{y}|\Phi_0^{N_A}\rangle, \quad (\text{S71})$$

$$7. |N\rangle = |\Theta_0\rangle|\Phi_{\mu>0}^{N_A}\rangle, |M\rangle = |\Theta_j^b\rangle|\Phi_0^{N_A}\rangle$$

$$A_{\mu,bj} = \langle\Phi_{\mu>0}^{N_A}|\hat{x}^\dagger\hat{y}|\Phi_0^{N_A}\rangle(xy|jb), \quad (\text{S72})$$

$$B_{\mu,bj} = \langle\Phi_{\mu>0}^{N_A}|\hat{x}^\dagger\hat{y}|\Phi_0^{N_A}\rangle(xy|bj), \quad (\text{S73})$$

$$8. |N\rangle = |\Theta_0\rangle|\Phi_{\mu>0}^{N_A}\rangle, |M\rangle = |\Theta_j\rangle|\Phi_\nu^{N_A+1}\rangle$$

$$A_{\mu,\nu j} = (-1)\langle\Phi_{\mu>0}^{N_A}|\hat{x}^\dagger\hat{y}|\Phi_0^{N_A}\rangle(xy|jz)\langle\Phi_0^{N_A}|\hat{z}|\Phi_\nu^{N_A+1}\rangle, \quad (\text{S74})$$

$$B_{\mu,\nu j} = (-1)\langle\Phi_{\mu>0}^{N_A}|\hat{x}^\dagger\hat{y}|\Phi_0^{N_A}\rangle(xy|zj)\langle\Phi_\nu^{N_A+1}|\hat{z}^\dagger|\Phi_0^{N_A}\rangle, \quad (\text{S75})$$

$$9. |N\rangle = |\Theta_0\rangle|\Phi_{\mu>0}^{N_A}\rangle, |M\rangle = |\Theta^b\rangle|\Phi_\nu^{N_A-1}\rangle$$

$$A_{\mu,b\nu} = \langle\Phi_{\mu>0}^{N_A}|\hat{x}^\dagger\hat{y}|\Phi_0^{N_A}\rangle(xy|zb)\langle\Phi_0^{N_A}|\hat{z}^\dagger|\Phi_\nu^{N_A-1}\rangle, \quad (\text{S76})$$

$$B_{\mu,b\nu} = \langle\Phi_{\mu>0}^{N_A}|\hat{x}^\dagger\hat{y}|\Phi_0^{N_A}\rangle(xy|bz)\langle\Phi_\nu^{N_A-1}|\hat{z}|\Phi_0^{N_A}\rangle, \quad (\text{S77})$$

$$10. |N\rangle = |\Theta_0\rangle|\Phi_{\mu>0}^{N_A}\rangle, |M\rangle = |\Theta_0\rangle|\Phi_{\nu>0}^{N_A}\rangle$$

$$A_{\mu,\nu} = \omega_{\mu}^{N_A} \delta_{\mu\nu}, \quad (\text{S78})$$

$$B_{\mu,\nu} = 0. \quad (\text{S79})$$

As is shown in the above expressions, \hat{H}_A needs to be diagonalized in three subspaces, with the number of active electrons N being N_A , $N_A + 1$ and $N_A - 1$, respectively, and three types of transition density matrices within the active space are required for constructing **A** and **B**:

$$\langle\Phi_{\mu}^{N_A+1}|\hat{x}^\dagger|\Phi_0^{N_A}\rangle, \quad \langle\Phi_{\mu}^{N_A-1}|\hat{x}|\Phi_0^{N_A}\rangle, \quad \langle\Phi_{\mu>0}^{N_A}|\hat{x}^\dagger\hat{y}|\Phi_0^{N_A}\rangle. \quad (\text{S80})$$

S3. COMPUTATIONAL DETAILS AND NUMERICAL RESULTS

A. Computational details

- RHF, CASSCF and SC-NEVPT2 results are obtained using the PySCF package[59].
- Molecular integrals and transition density matrices necessary for MR-RPA/SOSEX are computed using the PySCF package[59].
- For H_2^+ and H_2 with the cc-pVDZ basis set[60], the FCI results are used as references. For other molecules, where direct FCI calculations are infeasible, we use the *ab initio* spin-adapted DMRG results computed using the FOCUS package[64] as references. The bond dimensions D in DMRG used for HF and H_2O are 3000 and 4000, respectively, which provide numerically exact results. For N_2 and ScH, a larger D is needed, which is chosen to be 5000 with estimated errors below 0.01 mH and 0.1mH, respectively, for all the investigated inter-atomic distances.
- Dissociation energy is defined as the difference of energies between the dissociated limit and the minimum, $\Delta E = E(\text{dis}) - E(\text{min})$, where $E(\text{min})$ is obtained by a spline interpolation of the computed data.
- Non-parallel error (NPE) is computed as the difference between the maximal and minimal absolute deviations with respect to the FCI (or DMRG) results among the calculated points along the PEC.

B. SR-RPA implemented for comparison

For comparison, we also implemented the SR-RPA based on the RHF/ROHF orbitals. Specifically, the SR-RPA correlation energies for closed-shell molecules are obtained following the ‘plasmon’ formula as Eqs. (12) and (13), with **A** and **B** defined as

$$A_{ai,bj} = \delta_{ij}\delta_{ab}(\epsilon_a - \epsilon_i) + (ai|jb), \quad (\text{S81})$$

$$B_{ai,bj} = (ai|bj), \quad (\text{S82})$$

where $\{i, j, \dots\}$ and $\{a, b, \dots\}$ are RHF occupied and virtual spin-orbitals, respectively, and ϵ_a and ϵ_i are RHF orbital energies. For open-shell molecules, we used the following definition for **A**

$$A_{ai,bj} = \delta_{ij}F_{ab} - \delta_{ab}F_{ij} + (ai|jb), \quad (\text{S83})$$

where F_{ij} and F_{ab} are Fock matrix elements under spin-orbitals with the ROHF orbitals and density matrices. For H_2^+ , molecular orbitals are obtained by diagonalizing the core (kinetic plus nuclear attraction) terms of one-electron Hamiltonian.

C. Results for H_2^+ , H_2 , HF, ScH, H_2O , and N_2

Energies (in Hartree) computed with different methods using the cc-pVDZ basis set[60] can be found in Tables S1-S6. Dissociation energies ΔE , equilibrium bond distances R_{eq} , and non-parallel errors (NPEs) with respect to the DMRG results obtained by different methods using the cc-pVDZ basis set are compared in Table S7.

TABLE S1. Energies (in Hartree) for H_2^+ computed with different methods using the cc-pVDZ basis set. A CAS(1,1) active space is employed, which contains the orbital with the lowest orbital energy. Note that the ROHF results are exact for the one-electron system.

$R/\text{\AA}$	ROHF	SR-RPA	MR-RPA
0.5	-0.401 033	-0.411 325	-0.410 989
0.7	-0.551 432	-0.563 132	-0.562 678
0.8	-0.580 198	-0.592 576	-0.592 047
0.9	-0.594 390	-0.607 428	-0.606 811
1.0	-0.599 767	-0.613 459	-0.612 742
1.1	-0.599 772	-0.614 135	-0.613 301
1.3	-0.591 313	-0.607 139	-0.606 015
1.5	-0.578 095	-0.595 663	-0.594 149
2.0	-0.545 536	-0.568 917	-0.565 913
2.5	-0.524 118	-0.554 915	-0.549 698
3.0	-0.511 725	-0.550 516	-0.542 549
4.0	-0.501 864	-0.554 377	-0.540 821
5.0	-0.499 742	-0.561 778	-0.543 688
6.0	-0.499 353	-0.568 330	-0.546 580
7.0	-0.499 293	-0.573 770	-0.548 913
8.0	-0.499 284	-0.578 334	-0.550 760

TABLE S2. Energies (in Hartree) for H_2 computed with different methods using the cc-pVDZ basis set. A CAS(2,2) active space is employed, which contains the σ bonding orbital and its corresponding anti-bonding orbital.

$R/\text{\AA}$	RHF	MP2	SR-RPA	FCI
0.5	-1.048 800	-1.072 762	-1.090 547	-1.079 370
0.6	-1.106 892	-1.131 925	-1.150 104	-1.139 173
0.7	-1.126 924	-1.152 929	-1.171 328	-1.160 904
0.8	-1.127 000	-1.153 908	-1.172 366	-1.162 750
0.9	-1.116 391	-1.144 180	-1.162 557	-1.154 081
1.0	-1.100 153	-1.128 859	-1.147 042	-1.140 073
1.2	-1.061 112	-1.091 987	-1.109 522	-1.106 855
1.5	-1.002 192	-1.037 835	-1.053 890	-1.061 534
1.8	-0.950 939	-0.993 826	-1.007 678	-1.030 438
2.0	-0.921 908	-0.971 171	-0.982 998	-1.017 594
3.0	-0.826 447	-0.925 660	-0.915 609	-0.999 550
4.0	-0.782 198	-0.953 192	-0.898 197	-0.998 606
5.0	-0.762 044	-1.008 590	-0.897 178	-0.998 559
6.0	-0.751 715	-1.070 074	-0.900 120	-0.998 557
7.0	-0.745 197	-1.133 225	-0.903 668	-0.998 556
8.0	-0.740 452	-1.197 798	-0.907 086	-0.998 556
$R/\text{\AA}$	CASSCF	MR-RPA	MR-SOSEX	SC-NEVPT2
0.5	-1.061 149	-1.090 074	-1.075 745	-1.072 929
0.6	-1.121 408	-1.150 380	-1.136 073	-1.132 885
0.7	-1.143 977	-1.172 626	-1.158 531	-1.154 929
0.8	-1.146 973	-1.175 002	-1.161 271	-1.157 217
0.9	-1.139 684	-1.166 905	-1.153 631	-1.149 082
1.0	-1.127 199	-1.153 512	-1.140 743	-1.135 660
1.2	-1.097 155	-1.121 610	-1.109 848	-1.103 638
1.5	-1.056 125	-1.078 219	-1.067 661	-1.059 856
1.8	-1.028 006	-1.048 475	-1.038 642	-1.029 750
2.0	-1.016 299	-1.036 057	-1.026 492	-1.017 249
3.0	-0.999 507	-1.018 080	-1.008 827	-0.999 540
4.0	-0.998 603	-1.017 103	-1.007 855	-0.998 605
5.0	-0.998 556	-1.017 056	-1.007 805	-0.998 559
6.0	-0.998 556	-1.017 054	-1.007 805	-0.998 557
7.0	-0.998 556	-1.017 054	-1.007 805	-0.998 556
8.0	-0.998 556	-1.017 053	-1.007 805	-0.998 556

TABLE S3. Energies (in Hartree) for HF computed with different methods using the cc-pVDZ basis set. A CAS(2,2) active space is employed, which contains the σ bonding orbital and its corresponding anti-bonding orbital.

R/R_0 ($R_0 = 0.92\text{\AA}$)	RHF	SR-RPA	SR-SOSEX	DMRG ($D = 3000$)
0.5	-99.037 349	-99.247 510	-99.177 773	-99.226 582
0.7	-99.846 509	-100.065 122	-99.991 989	-100.045 505
0.8	-99.965 523	-100.187 394	-100.112 840	-100.168 712
0.9	-100.011 409	-100.236 299	-100.160 357	-100.218 668
1.0	-100.019 288	-100.247 051	-100.169 724	-100.230 595
1.1	-100.007 651	-100.238 156	-100.159 443	-100.223 039
1.3	-99.960 690	-100.196 387	-100.114 891	-100.184 769
1.5	-99.906 551	-100.147 392	-100.063 038	-100.141 062
2.0	-99.791 263	-100.046 705	-99.954 488	-100.064 761
2.5	-99.712 320	-99.985 346	-99.884 095	-100.037 268
3.0	-99.660 363	-99.952 042	-99.841 269	-100.030 649
4.0	-99.605 616	-99.929 457	-99.802 110	-100.028 894
5.0	-99.582 258	-99.928 426	-99.789 443	-100.028 801
R/R_0	CASSCF	MR-RPA	MR-SOSEX	SC-NEVPT2
0.5	-99.045 218	-99.247 139	-99.182 344	-99.217 296
0.7	-99.859 759	-100.065 515	-99.999 864	-100.037 387
0.8	-99.981 771	-100.188 955	-100.122 907	-100.161 545
0.9	-100.031 102	-100.239 402	-100.172 966	-100.212 514
1.0	-100.042 968	-100.251 927	-100.185 141	-100.225 299
1.1	-100.035 934	-100.244 971	-100.177 891	-100.218 263
1.3	-100.000 380	-100.207 680	-100.140 225	-100.179 693
1.5	-99.961 199	-100.164 728	-100.097 115	-100.134 262
2.0	-99.898 113	-100.091 086	-100.023 242	-100.054 029
2.5	-99.877 406	-100.065 490	-99.997 612	-100.025 955
3.0	-99.872 507	-100.059 323	-99.991 469	-100.019 335
4.0	-99.871 164	-100.057 630	-99.989 790	-100.017 564
5.0	-99.871 142	-100.057 593	-99.989 758	-100.017 523

TABLE S4. Energies (in Hartree) for ScH computed with different methods using the cc-pVDZ basis set. A CAS(4,4) active space is employed, which contains four σ orbitals with $4s(\text{Sc})$, $3d_{z^2}(\text{Sc})$, $4p_z(\text{Sc})$, and $1s(\text{H})$ characters.

R/R_0 ($R_0 = 1.7754\text{\AA}$)	RHF	SR-RPA	SR-SOSEX	DMRG ($D = 5000$)
0.5	-759.814 970	-760.075 719	-759.988 320	-760.072 540
0.7	-760.176 429	-760.443 046	-760.353 278	-760.441 998
0.8	-760.238 776	-760.504 323	-760.414 174	-760.504 011
0.9	-760.265 992	-760.530 390	-760.440 080	-760.531 006
1.0	-760.272 795	-760.536 115	-760.445 794	-760.537 945
1.1	-760.267 976	-760.530 204	-760.439 983	-760.533 548
1.3	-760.242 574	-760.502 830	-760.412 893	-760.510 792
1.5	-760.211 464	-760.470 236	-760.380 480	-760.485 791
2.0	-760.145 156	-760.402 671	-760.312 538	-760.455 003
2.5	-760.100 375	-760.362 400	-760.269 699	-760.452 157
3.0	-760.069 926	-760.342 145	-760.244 513	-760.452 048
4.0	-760.035 322	-760.336 211	-760.224 963	-760.451 755
5.0	-760.021 261	-760.342 303	-760.221 334	-760.451 720
R/R_0	CASSCF	MR-RPA	MR-SOSEX	SC-NEVPT2
0.5	-759.839 407	-760.077 704	-760.001 131	-760.037 822
0.7	-760.205 446	-760.447 312	-760.369 377	-760.407 394
0.8	-760.269 098	-760.509 164	-760.431 596	-760.469 129
0.9	-760.298 274	-760.536 231	-760.459 092	-760.495 850
1.0	-760.307 941	-760.543 399	-760.466 866	-760.502 526
1.1	-760.306 926	-760.539 359	-760.463 656	-760.498 037
1.3	-760.291 380	-760.517 241	-760.443 517	-760.475 540
1.5	-760.272 084	-760.492 899	-760.420 786	-760.451 464
2.0	-760.247 383	-760.463 417	-760.392 866	-760.424 320
2.5	-760.247 097	-760.463 243	-760.392 480	-760.422 611
3.0	-760.247 364	-760.463 403	-760.392 656	-760.422 679
4.0	-760.247 415	-760.463 080	-760.392 446	-760.422 412
5.0	-760.247 408	-760.463 027	-760.392 407	-760.422 368

TABLE S5. Energies (in Hartree) for the symmetric dissociation of H₂O computed with different methods using the cc-pVDZ basis set. A CAS(4,4) active space is employed, which contains two σ bonding orbitals and their corresponding anti-bonding orbitals. The H–O–H angle is set to 104.5°.

R/R_0 ($R_0 = 0.98\text{\AA}$)	RHF	SR-RPA	SR-SOSEX	DMRG ($D = 4000$)
0.5	-74.337 841	-74.539 306	-74.471 331	-74.518 465
0.7	-75.735 198	-75.952 082	-75.877 584	-75.932 779
0.8	-75.940 396	-76.162 834	-76.085 709	-76.144 987
0.9	-76.016 417	-76.243 882	-76.164 255	-76.227 878
1.0	-76.024 735	-76.257 168	-76.174 993	-76.243 453
1.1	-75.998 350	-76.235 872	-76.151 032	-76.225 042
1.3	-75.905 125	-76.153 398	-76.062 791	-76.151 054
1.5	-75.801 910	-76.061 905	-75.964 944	-76.073 200
2.0	-75.586 475	-75.880 576	-75.765 811	-75.951 410
2.5	-75.473 027	-75.741 577	-75.629 940	-75.916 998
3.0	-75.438 091	-75.720 454	-75.596 892	-75.911 884
4.0	-75.415 806	-75.721 976	-75.584 967	-75.910 369
5.0	-75.406 815	-75.727 292	-75.583 051	-75.910 307
R/R_0	CASSCF	MR-SOSEX	MR-RPA	SC-NEVPT2
0.5	-74.365 099	-74.542 543	-74.485 672	-74.505 417
0.7	-75.767 150	-75.954 163	-75.893 578	-75.915 535
0.8	-75.978 368	-76.165 882	-76.105 101	-76.127 744
0.9	-76.061 334	-76.248 833	-76.187 902	-76.210 959
1.0	-76.077 771	-76.264 975	-76.203 849	-76.227 072
1.1	-76.060 842	-76.247 561	-76.186 147	-76.209 332
1.3	-75.991 498	-76.176 226	-76.114 052	-76.136 527
1.5	-75.920 454	-76.100 826	-76.038 148	-76.058 740
2.0	-75.816 722	-75.983 211	-75.921 124	-75.935 722
2.5	-75.791 230	-75.950 743	-75.889 741	-75.902 153
3.0	-75.787 125	-75.945 102	-75.884 342	-75.896 441
4.0	-75.786 129	-75.943 705	-75.883 005	-75.895 061
5.0	-75.786 072	-75.943 625	-75.882 933	-75.894 978

TABLE S6. Energies (in Hartree) for N_2 computed with different methods using the cc-pVDZ basis set. A CAS(6,6) active space is employed, which contains one σ bonding orbital, two π bonding orbitals and their corresponding anti-bonding orbitals.

R/R_0 ($R_0 = 1.095\text{\AA}$)	RHF	SR-RPA	SR-SOSEX	DMRG ($D = 5000$)
0.5	-104.709 478	-104.944 935	-104.862 717	-104.921 795
0.7	-108.201 116	-108.467 782	-108.376 209	-108.452 882
0.8	-108.718 875	-109.003 032	-108.905 362	-108.993 482
0.9	-108.918 011	-109.219 710	-109.115 898	-109.217 148
1.0	-108.954 475	-109.274 227	-109.164 153	-109.280 519
1.1	-108.911 368	-109.250 078	-109.133 492	-109.267 178
1.3	-108.741 863	-109.121 579	-108.990 939	-109.166 253
1.5	-108.591 863	-108.917 784	-108.799 612	-109.067 669
2.0	-108.426 530	-108.732 517	-108.608 993	-108.971 457
2.5	-108.340 021	-108.664 534	-108.529 536	-108.962 430
3.0	-108.283 688	-108.631 855	-108.484 625	-108.960 980
4.0	-108.228 319	-108.614 917	-108.448 089	-108.960 280
5.0	-108.210 453	-108.618 005	-108.440 320	-108.960 235
R/R_0	CASSCF	MR-RPA	MR-SOSEX	SC-NEVPT2
0.5	-104.755 679	-104.940 086	-104.876 594	-104.894 211
0.7	-108.274 241	-108.466 240	-108.400 490	-108.418 144
0.8	-108.809 885	-109.007 164	-108.939 082	-108.958 445
0.9	-109.029 622	-109.231 449	-109.161 117	-109.182 183
1.0	-109.089 748	-109.295 442	-109.223 038	-109.245 821
1.1	-109.073 550	-109.282 649	-109.208 336	-109.232 889
1.3	-108.967 708	-109.182 427	-109.105 082	-109.132 799
1.5	-108.866 500	-109.084 087	-109.005 885	-109.034 361
2.0	-108.780 465	-108.987 506	-108.914 277	-108.937 432
2.5	-108.777 293	-108.979 240	-108.907 177	-108.929 421
3.0	-108.777 143	-108.978 090	-108.906 231	-108.928 350
4.0	-108.776 848	-108.977 513	-108.905 719	-108.927 790
5.0	-108.776 828	-108.977 478	-108.905 685	-108.927 752

TABLE S7. Dissociation energies ΔE , equilibrium bond distances R_{eq} , and non-parallel errors (NPEs) with respect to the DMRG results obtained by different methods using the cc-pVDZ basis set.

Molecule	Method	ΔE (mH)	R_{eq} (Å)	NPE (mH)
HF	CASSCF	171.8	0.920	29.97
	MR-RPA	194.3	0.922	8.78
	MR-SOSEX	195.4	0.920	6.76
	SC-NEVPT2	207.8	0.923	6.55
	DMRG	201.8	0.919	/
ScH	CASSCF	61.1	1.836	32.24
	MR-RPA	80.4	1.781	6.20
	MR-SOSEX	74.5	1.794	13.31
	SC-NEVPT2	80.2	1.773	6.17
	DMRG	86.2	1.776	/
H ₂ O	CASSCF	292.0	0.966	42.38
	MR-RPA	321.7	0.965	12.85
	MR-SOSEX	321.3	0.965	12.72
	SC-NEVPT2	332.5	0.965	4.20
	DMRG	333.7	0.963	/
N ₂	CASSCF	313.9	1.114	35.05
	MR-RPA	319.6	1.120	4.93
	MR-SOSEX	318.6	1.117	16.58
	SC-NEVPT2	319.7	1.120	7.45
	DMRG	321.8	1.119	/